There are amendments to this paper

Structure and assembly of calcium homeostasis modulator proteins

Johanna L. Syrjanen[1], Kevin Michalski[1], Tsung-Han Chou [1], Timothy Grant[2], Shanlin Rao[3,4], Noriko Simorowski[1], Stephen J. Tucker [3], Nikolaus Grigorieff [2,5] and Hiro Furukawa [1]*

The biological membranes of many cell types contain large-pore channels through which a wide variety of ions and metabolites permeate. Examples include connexin, innexin and pannexin, which form gap junctions and/or bona fide cell surface channels. The most recently identified large-pore channels are the calcium homeostasis modulators (CALHMs), through which ions and ATP permeate in a voltage-dependent manner to control neuronal excitability, taste signaling and pathologies of depression and Alzheimer's disease. Despite such critical biological roles, the structures and patterns of their oligomeric assembly remain unclear. Here, we reveal the structures of two CALHMs, chicken CALHM1 and human CALHM2, by single-particle cryo-electron microscopy (cryo-EM), which show novel assembly of the four transmembrane helices into channels of octamers and undecamers, respectively. Furthermore, molecular dynamics simulations suggest that lipids can favorably assemble into a bilayer within the larger CALHM2 pore, but not within CALHM1, demonstrating the potential correlation between pore size, lipid accommodation and channel activity.

Permeation of ions and/or substrates, such as ATP, through CALHM proteins is fundamental to the physiology of depression[1] and cognition[2], as well as to the pathology of Alzheimer's disease[3]. The CALHM family comprises six members, CALHM1–6 (sequence homology ~30–50%), amongst which CALHM1 has been the most extensively studied to date. CALHM1 forms a channel that conducts ATP[4] and ions, including Ca^{2+}, Na^+, K^+ and Cl^-, in a voltage-dependent manner[5]. A single-nucleotide polymorphism within the *calhm1* gene that results in a Pro86Leu alteration was reported to be a risk factor for early onset of Alzheimer's disease[3] and, at the cellular level, this mutation has been shown to promote deposition of amyloid beta, a hallmark of Alzheimer's disease[6]. Later studies showed that CALHM1 proteins are expressed in type II taste-bud cells to mediate ATP efflux, which results in purinergic signaling for sweet, bitter and umami taste sensations[4]. ATP efflux from CALHM1 was also shown to control ciliary beat frequency for mucociliary clearance in airways[7]. More recently, the function of CALHM2 proteins expressed in astrocytes has been linked to depression[1] and implicated as playing a role in glial–neuronal functions[1]. While CALHM3 has been shown to form heteromeric channels with CALHM1 (ref. [8]), the functions and biological roles of the remaining members, CALHM4–6, are currently unknown. The *calhm* genes are conserved throughout vertebrates and nonvertebrates. Furthermore, CALHM1 from *Caenorhabditis elegans* has been shown to possess similar ion-channel properties to those of human CALHM1 (hCALHM1)[9], demonstrating functional conservation throughout diverse species.

Topological prediction of the CALHM protein family has been difficult. Originally, CALHM was suggested to have similar membrane topology to *N*-methyl-D-aspartate receptors (NMDARs)[3] and later to hemichannel and gap junction proteins, including connexin and innexin, on the basis of secondary structure prediction and comparison[5]. The CALHM family members have no primary sequence homology with NMDARs or any of the hemichannels and gap junction protein families mentioned, thus making it difficult to design functional experiments to address mechanisms. Overall, despite playing critical roles in human physiology and pathology, the structure and function of CALHM proteins at the molecular level remains unclear. Here, we show structures of two CALHM family members, CALHM1 and CALHM2, in lipid nanodiscs. Protomers of both CALHM1 and CALHM2 harbor four transmembrane domains and a long cytoplasmic helix, which do not resemble the known structures of other channels, including connexin, innexin and NMDARs. Despite belonging to the same protein family, CALHM1 and CALHM2 form channels with distinct oligomeric states, octamer and undecamer, respectively. Molecular dynamics simulation shows that the undecamer assembly in CALHM2 can stably accommodate lipids in its hydrophobic channel, whereas the octamer assembly of CALHM1 cannot, suggesting the possibility of lipid accommodation as a means to regulate channel function.

Results

Preparation of CALHM proteins. In this study we focused on the two major family members, CALHM1 and CALHM2, that are involved in controlling the excitability of neurons[1,2]. We first conducted expression screening of CALHM orthologs using fluorescence-coupled size-exclusion chromatography[10], from which we concluded that chicken CALHM1 (chCALHM1) and hCALHM2 show a homogeneity in protein size that is suitable for structural analysis. The primary sequences of chCALHM1 and hCALHM1 have 67.7% identity and 80.2% similarity overall, and 81.4% identity and 93.8% similarity within the transmembrane domains (TMDs) (Supplementary Fig. 1). chCALHM1 also contains Asp 120, the equivalent residue of which in hCALHM1 (Asp 121) has been shown to be critical for its ion-channel activity[5] (Supplementary Fig. 1). Indeed, our patch-clamp electrophysiology results show

[1]WM Keck Structural Biology Laboratory, Cold Spring Harbor Laboratory, Cold Spring Harbor, NY, USA. [2]Janelia Research Campus, Howard Hughes Medical Institute, Ashburn, VA, USA. [3]Department of Biochemistry, University of Oxford, Oxford, UK. [4]Clarendon Laboratory, Department of Physics, University of Oxford, Oxford, UK. [5]RNA Therapeutics Institute, University of Massachusetts Medical School, Worcester, MA, USA. *e-mail: furukawa@cshl.edu

that chCALHM1 has similar functional properties to hCALHM1, including voltage sensitivity, calcium-sensitive inhibition and channel blockade by ruthenium red (Fig. 1a,b). Both chCALHM1 and hCALHM2 proteins were recombinantly expressed in *Sf*9 insect cells infected with the respective recombinant baculoviruses[11], purified and reconstituted into lipid nanodiscs before vitrification for the cryo-EM study (Extended Data Fig. 1; also see Methods).

Cryo-EM structure of CALHM1. We solved the structure of chCALHM1 using single-particle cryo-EM analysis at an overall resolution of 3.63 Å (Fig. 1c–e, Extended Data Figs. 2 and 3 and Table 1), as assessed by Fourier shell correlation (FSC)[12,13]. The cryo-EM structure was solved in the presence of EDTA to remove free divalent ions such as calcium, and therefore likely mimics the active state. The cryo-EM density of the extracellular domain, the four TMD helices and the cytoplasmic helices (CTHs) were of sufficient quality to conduct de novo modeling between residues 26–79, 91–137 and 151–247, altogether spanning 198 out of 342 amino acids. Most of the missing density is in the carboxy-terminal region after the CTH, where 72 out of 94 residues are predicted to be unstructured by a secondary structure analysis[14]. The structure confirms the previous prediction that CALHM1 harbors four TMDs with the amino and carboxy termini facing the cytoplasm[15]. The cryo-EM density for TMD1, which faces the pore, is weaker compared to the other three TMDs, indicating the presence of conformational flexibility. Our current structure clearly shows octameric assembly, with a pore-like structure in the middle of the oligomer (Fig. 1c,d). The assembly is mediated mainly by interactions between TMD2 and TMD4, between TMD1 and TMD3 and between the 40-residue-long CTHs of neighboring subunits (Fig. 2). The octameric assembly shown in our high-resolution cryo-EM structure differs from a previous study suggesting hexameric assembly of CALHM1 on the basis of Blue native–PAGE and photobleaching of hCALHM1-EGFP constructs[15]. Nevertheless, the subunit interface residues are highly conserved between chCALHM1 and hCALHM1, strongly implying preservation of oligomeric mechanisms (Supplementary Figs. 1 and 2; 88.5% identity and 100% similarity over 35 residues in TMDs and CTH). In the present study, two- and three-dimensional (2D or 3D) classification did not support the presence of other oligomeric species, such as hexamers. Furthermore, there is clear density for TMD4, CTH and the TMD4–CTH linker (Extended Data Fig. 3), indicating that the interprotomer interaction mode is well defined and stable. Some unresolved density extends from TMD1 toward the middle of the channel at the cytoplasmic side, likely representing the amino-terminal residues in multiple conformations (Extended Data Fig. 4). In CALHM1 from human and *C. elegans*, the first nine residues have been shown to alter voltage sensitivity[16], thus, we suggest that these voltage-sensing residues are located in the inner pore within the membrane-spanning region (Extended Data Fig. 4). The pore diameter measured on the basis of the above cryo-EM density is 19.5 Å, which is similar to the previously estimated diameter of 14 Å based on a dye-permeation assay and electrophysiological measurement of permeation of tetralkylammonium cation[15].

The only other octameric channel reported to date is innexin[17], however, it does not share similar features with chCALHM1 in its pattern of oligomeric assembly. Furthermore, contrary to a previous

suggestion, there is no similarity in the membrane topology, structure and oligomeric assembly pattern of chCALHM1 to NMDARs[3], which contain three TMDs and a re-entrant loop, and form heterotetramers[18,19]. Importantly, the structural comparison of monomers demonstrated that chCALHM1 does not resemble other four-transmembrane-channel proteins, including connexin[20], innexin[17] and the volume-regulated anion channel (LRRC8)[21,22] (Fig. 1f).

A key residue known to modulate CALHM1 ion permeability and calcium sensitivity, Asp 120 (Asp 121 in hCALHM1)[5], is located in TMD3, at the interface with the neighboring subunit (Fig. 2a–c). Although in chCALHM1 each of the Asp 120 residues face the inner pore, they do not appear to participate in pore formation directly, as they are distant from each other (~20 Å between the Cα positions of the neighboring Asp 120 residues). Instead, Asp 120 may facilitate intersubunit interactions that stabilize channel assembly (Fig. 2c). Alteration of another key residue in hCALHM1 (Pro86Leu) has also previously been shown to be a risk factor for the age of onset of Alzheimer's disease in selected populations[3], and, although the equivalent residue in chCALHM1 is Gln 85, it is clear that this residue is located in the disordered loop between TMD2 and TMD3. Consistent with this location, which faces the cytoplasm and is not part of the channel pore (Fig. 2a,b; asterisks), the Pro86Leu change in hCALHM1 has previously been shown not to alter channel activity[5]. Instead, the mechanisms underlying the association of this mutation with Alzheimer's disease pathology may involve other factors, such as protein–protein interactions involving this loop and subsequent cell-signaling events that regulate the level of amyloid beta[23].

Cryo-EM structure of CALHM2. CALHM2 has a moderately high sequence similarity to CALHM1 within the predicted TMD domains (35% identity and 56% similarity between hCALHM1 and hCALHM2, and 37% identity and 55% similarity between chCALHM1 and hCALHM2; Supplementary Fig. 2), yet, unlike CALHM1, it does not show voltage-dependent ion-channel activities (Fig. 1a)[8]. Thus, we wondered what structural features of CALHM1 and CALHM2 might be responsible for this functional difference. To permit an extensive comparison, we conducted a structural analysis of the human CALHM2 protein by implementing a similar protocol to that used above for chCALHM1 (Extended Data Fig. 1; also see Methods). Single-particle cryo-EM analysis of the hCALHM2 sample in the absence of calcium resulted in one major 3D class at 3.48-Å resolution, as assessed by FSC (Extended Data Figs. 5 and 6 and Table 1). As in the case of chCALHM1, the hCALHM2 protomer contains four TMDs and the long CTH that is the signature of the CALHM family (Fig. 3a–c). The orientations of the four TMD helices in hCALHM2 are also similar to those of chCALHM1 and are unrelated to connexin, innexin or the volume-regulated anion channel (Fig. 3d). However, the profound structural difference between chCALHM1 and hCALHM2 is that the oligomeric state of hCALHM2 is an undecamer (Fig. 3a,b). As in chCALHM1, the oligomeric assembly of hCALHM2 is mediated by interactions between TMD2 and TMD4, between TMD1 and TMD3 and between the CTHs of the neighboring subunits (Extended Data Fig. 7). However, the fundamental difference is in the angle between TMD4 and the CTH, which is controlled by the linker sequence

Fig. 1 | Structure and function of chCALHM1. a, Currents recorded for hCALHM1 and chCALHM1 with voltage steps from −100 to +100 mV in 10-mV increments in the presence and absence of extracellular calcium. The current of chCALHM1 can be blocked by 0.02 mM ruthenium red (RuR), as previously shown for hCALHM1. No voltage-dependent current compared to mock transfected cells was observed for hCALHM2, consistent with the previous report[8]. **b,** G–V plot of chCALHM1 and hCALHM1 with no CaCl₂ (right panel in **a**). Error bars represent s.e.m. for six individual patches (n = 6) for hCALHM1 and seven (n = 7) for chCALHM1. **c,d,** Cryo-EM density (**c**) and atomic models (**d**) of chCALHM1 viewed from the side of the membrane, the extracellular region and the cytoplasm. **e,** Ribbon (left) and schematic (right) representations of the chCALHM1 protomer. The TMDs are colored as blue, cyan, green and yellow for TMDs 1, 2, 3 and 4, respectively. Dashed lines represent regions that are not visible in our structure. **f,** Protomers of chCALHM1, connexin (CX26) (ref. [20]), innexin[17] and LRRC8A[21]. The TMDs are colored as in **e** for comparison. Data for the graph in **b** are available as source data.

that tethers these two helices together (TMD–CTH linker; Fig. 3d). Consequently, the sites of inter-CTH interactions are different between chCALHM1 and hCALHM2. This linker sequence differs between CALHM family members, suggesting that CALHM4–6 may also

have distinct oligomeric states (Supplementary Fig. 2). It is interesting to note that CALHM1 and CALHM3 have similar linker sequences and are known to form heteromers[8]. Nevertheless, the undecamer channel assembly observed in hCALHM2 is unprecedented.
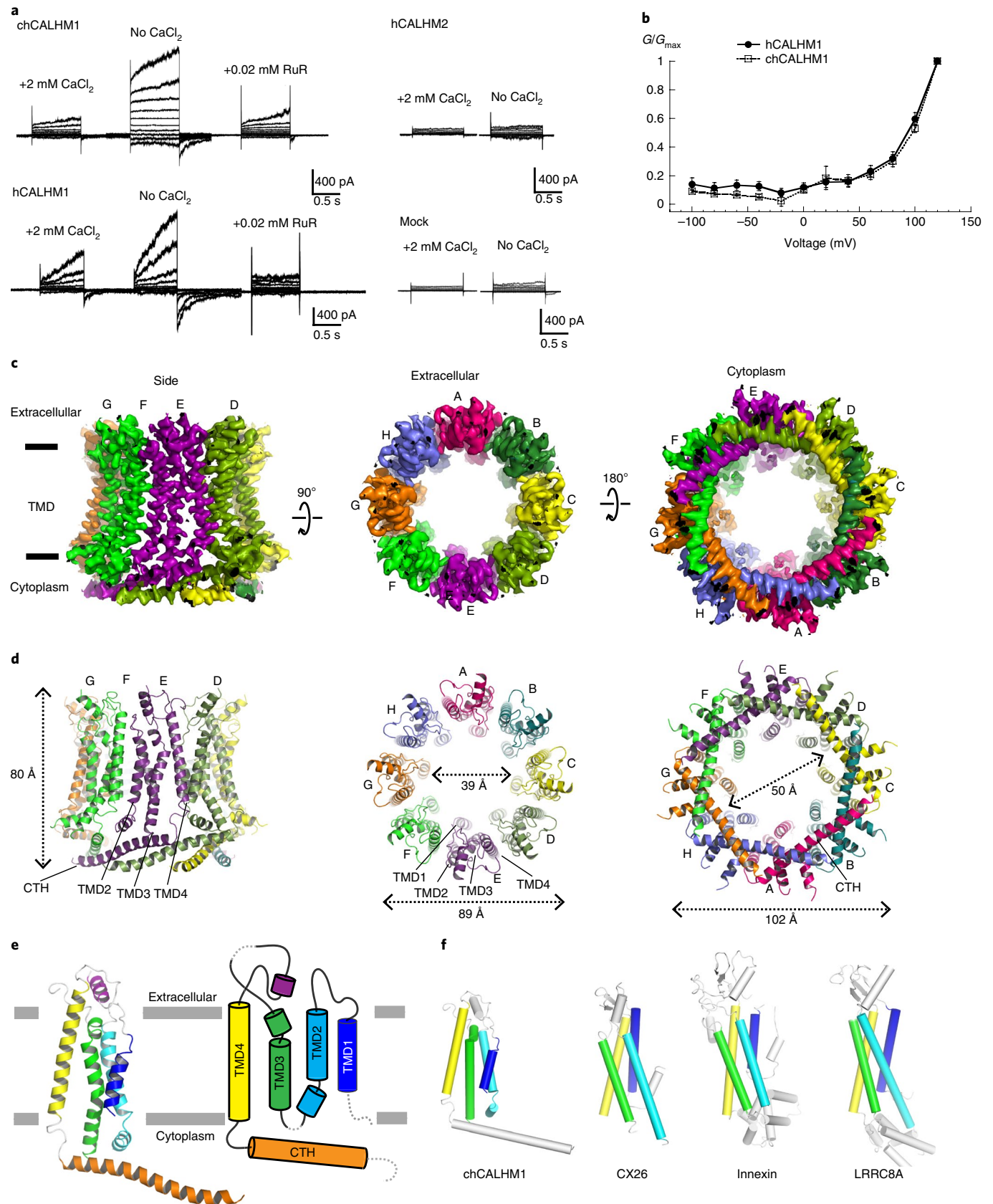
Table 1 | Cryo-EM data collection, refinement and validation statistics

	chCALHM1 (EMD-21143, PDB 6VAM)	hCALHM2 (EMD-21141, PDB 6VAK)	hCALHM2 gap junction (EMD-21140, PDB 6VAI)	chCALHM1–hCALHM2 chimera (EMD-21142, PDB 6VAL)
Data collection and processing				
Magnification	130,000	130,000	130,000	130,000
Voltage (kV)	300	300	300	300
Electron exposure (e⁻/Å²)	70	70	70	57.2
Defocus range (μm)	1.5–3.0	1.2–2.8	1.5–3.0	1.4–2.8
Pixel size (Å)	1.06	1.06	1.06	1.06
Symmetry imposed	C8	C11	D11	C11
Initial particle images (no.)	533,665	331,726	119,211	397,362
Final particle images (no.)	308,916	104,755	28,657	123,664
Map resolution (Å)	3.63	3.48	3.68	3.87
FSC threshold	0.143	0.143	0.143	0.143
Map resolution range (Å)	3.0–6.0	3.0–6.0	3.0–6.0	3.0–6.0
Refinement				
Initial model used (PDB code)	De novo	De novo	6VAK	6VAM/6VAK
Model resolution (Å)	3.92	3.63	3.79	4.32
FSC threshold	0.5	0.5	0.5	0.5
Map sharpening B factor (Å²)	−150	−90	−90	−90
Model composition				
Nonhydrogen atoms	13,312	22,781	45,584	21,615
Protein residues	1,712	2,292	5,784	2,827
Ligands	0	0	0	0
B factors (Å²)				
Protein	85.99	43.91	38.29	101.43
r.m.s. deviations				
Bond lengths (Å)	0.003	0.007	0.005	0.005
Bond angles (°)	0.603	0.746	0.678	0.728
Validation				
MolProbity score	1.70	2.13	1.99	1.90
Clashscore	6.08	8.72	8.94	9.19
Poor rotamers (%)	0	1.97	0.96	1.02
Ramachandran plot				
Favored (%)	94.71	93.28	91.34	94.02
Allowed (%)	5.29	6.72	8.66	5.98
Disallowed (%)	0	0	0	0
Cβ deviation	0	0	0	0
EMRinger score	1.83	2.73	3.11	2.18
CαBLAM outlier (%)	3.47	3.79	2.70	2.04

Therefore, to validate the physiological relevance of this undecamer assembly in the membrane environment, we conducted a series of disulfide-based intersubunit cross-linking experiments (Fig. 3e). Based on the structure, we substituted residues in the intersubunit interface at the extracellular side of TMD2 and TMD4 (Arg 52/Tyr 182) and at the CTHs (Asn 226/Arg 240) with cysteines (Fig. 3e), subjected the mutants to SDS–PAGE and detected bands by western blot in the presence and absence of a reducing agent. In the case of the CTH mutants located in the cytoplasm, we facilitated disulfide bond formation by the addition of copper phenanthroline to the membrane fraction. In the non-reducing condition we observed a high molecular weight band around 460 kDa. Monomer bands were exclusively observed in the reducing condition, indicating

that the band shift in the non-reducing condition is mediated by disulfide bonding between the engineered cysteines (Fig. 3e). This result shows that the oligomeric assembly observed in the cryo-EM structure is consistent with its physiological state in the membrane.

Cytoplasmic domain governs oligomeric state. To test our structure-based hypothesis that the interactions between the CTHs control the oligomeric state of CALHMs, we made a chimeric construct of chCALHM1 TMDs and hCALHM2 cytoplasmic domains (CALHM1–CALHM2) and analyzed the oligomeric state by solving the cryo-EM structure in lipid nanodiscs, as was done in chCALHM1 and hCALHM2. Our cryo-EM structure at 3.9-Å resolution unambiguously showed an undecamer assembly
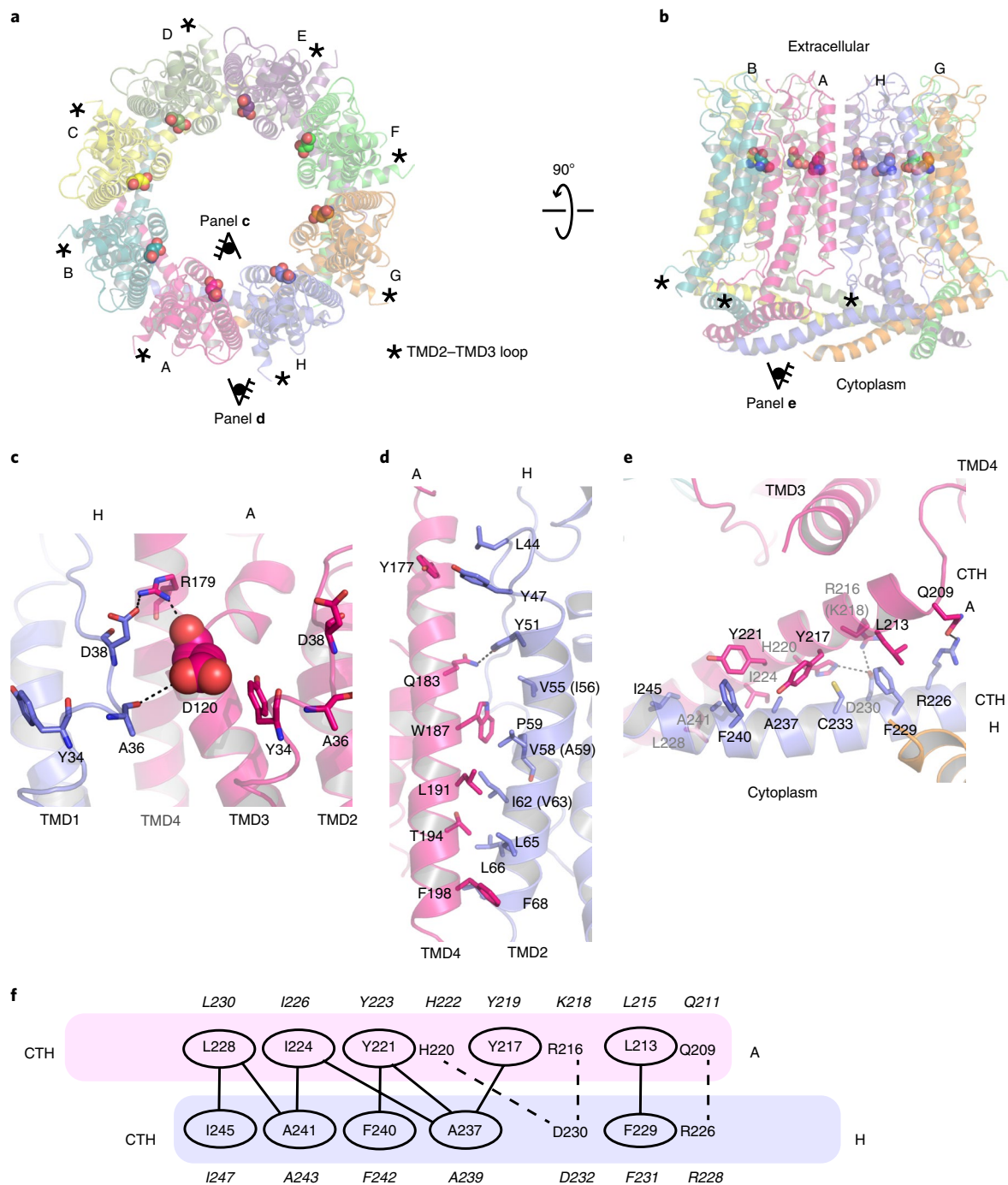
Fig. 2 | Intersubunit interface of chCALHM1. a,b, The chCALHM1 structure viewed from the top of the extracellular region (**a**) and from the side of the membrane (**b**). The Asp 120 residues that are critical for calcium sensitivity and ion permeation are shown as spheres. **c,** Asp 120 (sphere) and surrounding residues (sticks) form polar interactions to mediate intersubunit interactions. **d,e,** The intersubunit interactions between TMD2 and TMD4 (**d**) and CTHs (**e**). **f,** The schematic presentation of the interactions between two CTHs (magenta and slate blue). Polar and van der Waals interactions mediated by hydrophobic residues (ovals) are shown as dashed and solid lines, respectively. The residues in italic are the equivalent ones in hCALHM1.

that was similar, in principle, to the one observed in hCALHM2 (root mean square deviation (r.m.s.d.) = 2.83 Å over 2,386 aligned residues) (Fig. 4a and Extended Data Fig. 8). This demonstrates that replacing the cytoplasmic domain of chCALHM1 with that of hCALHM2 converts the oligomeric state of chCALHM1 from an octamer to an undecamer. The major structural determinants for the interprotomer interactions are TMD2–TMD4 and CTHs, as in the case of chCALHM1 and hCALHM2 (Fig. 4b,c). Consistent with

the undecamer assembly, the angle between TMD4 and CTH of CALHM1–CALHM2 is similar to that of hCALHM2, but not chCALHM1 (Fig. 4d). Moreover, the mode of inter-CTH interaction is similar between CALHM1–CALHM2 (Fig. 4c) and hCALHM2 (Extended Data Fig. 7e,f), implying that the TMD4–CTH linker and inter-CTH interactions govern the oligomeric state. Overall, our result demonstrates a proof-of-principle that the oligomeric state of CALHM1 can be manipulated by altering the cytoplasmic domain.

Cryo-EM structure of CALHM2 gap junction. One noteworthy observation is that the hCALMH2 undecamer dimerizes to form a 22-mer that is reminiscent of a gap junction in the presence of 1 mM $CaCl_2$ under cryo-EM conditions (Extended Data Figs. 9 and 10). Our 22-mer structure, solved at a resolution of 3.68 Å, showed high structural similarity to the undecamer structure (r.m.s.d. = 0.853 Å over 265 residues), indicating that calcium did not alter the overall protein architecture. The gap junction formation is mediated by His 147 and His 152 in the apposed hemichannels and possibly by Glu 145, which are located in the extracellular loop between TMD3 and TMD4 (Extended Data Fig. 10b, lower panel). The cryo-EM density between His 147 and His 152 is continuous, potentially implying that a divalent cation may be present to mediate an interaction between these two histidines, along with Glu 145. Under this condition, EDTA was not included, thus a trace amount of divalent ions, such as zinc ions, may be present in the sample. However, inclusion of 0.1 mM $ZnCl_2$ does not oligomerize hCALHM2 to a 22-mer assembly in solution, as observed by the identical peak retention time in size-exclusion chromatography (data not shown). It is therefore unclear if the 22-mer observed by cryo-EM exists under physiological conditions or whether the gap junction formation of hCALHM2 requires additional factors in solution.

Properties of channel pores. Further structural inspection revealed that the majority of the channel-lining residues (TMDs 1 and 3) in chCALHM1 are hydrophilic (Fig. 5a,b), whereas those in similar positions in hCALHM2 are hydrophobic (Fig. 5c–e). Thus, we speculated that hydrophobic molecules, lipids for example, may be favorably placed in this hydrophobic channel structure of hCALHM2. In hCALHM2, we observe amorphous density in the middle of the undecamer assembly, which is discontinuous from the density for proteins (Fig. 5f). In chCALHM1, the density in the middle of the octamer is stronger, more ordered and continuous from TMD1 (Extended Data Fig. 4). Therefore, the features of the extra cryo-EM density in the middle of the oligomeric assemblies appear to be distinct between chCALHM1 and hCALHM2. To assess if the undecamer channel structure in hCALHM2 can accommodate lipids in the middle, we conducted molecular dynamics simulations of chCALHM1 and hCALHM2 in the presence of 1-palmitoyl-2-oleoyl-*sn*-glycero-3-phosphocholine (POPC) (Fig. 5g,h). Coarse-grained structural models[24] of chCALHM1 and hCALHM2 were mixed with POPC lipids and allowed to self-assemble into bilayers[25]. During replicates of 500-ns simulations, a membrane bilayer formed around both proteins within the first 100 ns, with a number of lipids inside the channel pore. In hCALHM2, the central pore lipids were oriented with a bilayer-like configuration that remained stable, both in simulations of the protein–membrane systems on conversion into their corresponding atomistic representation, as well as in further, extended coarse-grained simulations (up to 5 μs per replicate) (Fig. 5h). By contrast, although phospholipids could also be accommodated within the smaller chCALHM1 pore, they did not assemble into clearly defined or stable inner and upper leaflets (Fig. 5h).

These simulations imply that the hydrophobicity and larger undecamer assembly of hCALHM2 may favor accommodation of lipid molecules, which prevent ion permeation.

Discussion

Our high-resolution structures of CALHM1 and CALHM2 and structural comparison offer insights into assembly patterns and function of the CALHM protein family. The protomers of CALHM1 and CALHM2 have similar structural architectures, including four TMDs and a long CTH in the cytoplasmic face, which are unique to this protein family. However, CALHM1 and CALHM2 protomers assemble as an octamer and undecamer, respectively, which marks an unusual case where different members of the same channel family form an assembly with distinct oligomeric states. These distinct patterns of channel assembly appear to be mediated by the unique modes of interaction between the CTHs. The structures in the current study were solved in the absence of voltage and in the presence of EDTA to remove divalent cations, which have been previously shown to inhibit the CALHM1 ion channel. Therefore, the chCALHM1 structure likely represents the active state; however, one cannot exclude the possibility that in the presence of voltage the channel may undergo further conformational transitions.

The oligomeric states of the CALHM1 and CALHM2 structures in our study were different from the hexameric assembly previously suggested for CALHM1 by Blue native–PAGE and a fluorescence-quenching assay of the EGFP-fused CALHM1 (ref. [15]). While our cryo-EM structures show octamer and undecamer assemblies for CALHM1 and CALHM2, respectively, we do not rule out the possibility that they can also exist in different oligomeric states. The interpromoter interfaces involve only neighboring promoters and, thus, there is a chance that large conformational changes within protomers may trigger different oligomeric assemblies. An example of such a case is calcium/calmodulin-dependent kinase II (CaMKII), where active and inactive protomers can shuffle and form either 12-mers or 14-mers interchangeably[26]. Under the experimental conditions in our current study (no divalent cations and samples in lipid nanodiscs), we did not observe any evidence of other oligomeric assembly by 2D or 3D classification. Furthermore, there is clear density for the linker between TMD4 and CTH in both CALHM1 and CALHM2 (Extended Data Figs. 3 and 6), indicating that the intrinsic structure of the linker is well ordered, and specific interactions between the CTHs are the major determinant for the observed oligomeric states. Supporting this hypothesis is our result that the oligomeric state of chCALHM1 can be converted from octamer to undecamer by substituting its cytoplasmic domain with that of hCALHM2 (Fig. 4). The structure of this chimeric construct, CALHM1–CALHM2, shows a similar TMD4–CTH angle and mode of inter-CTH interactions to those observed in hCALHM2 (Figs. 3d and 4c,d and Extended Data Fig. 7e,f). While we have not converted hCALHM2 from undecamer to octamer using the reverse approach at this point, our experimental results strongly support the role of the TMD4–CTH linker and the inter-CTH interactions in defining oligomeric states.

Fig. 3 | Structure and function of hCALHM2. a,b, Cryo-EM density (**a**) and atomic models (**b**) of hCALHM2 viewed from the side of the membrane, the extracellular region and the cytoplasm. **c,** Ribbon (left) and schematic (right) representations of the hCALHM2 protomer. The TMDs are colored as blue, cyan, green and yellow for TMDs 1, 2, 3 and 4, respectively. Dashed lines represent regions that are not visible in our structure. CT, carboxy terminus; NT, amino terminus. **d,** Superposition of the TMDs of the chCALHM1 (in cyan) and the hCALHM2 (in magenta) viewed from the side of the membrane (left) and the cytoplasm (right). r.m.s.d. of superposition is 1.1 Å over 105 Cα positions. **e,** Cysteine changes, Tyr182Cys/Arg52Cys or Asn226Cys/Arg240Cys (spheres), were introduced at the subunit interfaces to assess the formation of intersubunit disulfide cross-linking (left). Anti-1D4 western blots (right) of SDS–PAGE show band shifts for Tyr182Cys/Arg52Cys and Asn226Cys/Arg240Cys (arrow 1). Tyr182Cys/Arg52Cys forms disulfide bonds without copper phenanthroline. Formation of disulfide bonds for Asn226Cys/Arg240Cys requires copper phenanthroline treatment before (Asn226Cys/Arg240Cys memb) or after detergent solubilization. The wild-type (WT) hCALHM2 protein runs as a monomer under these conditions (arrow 2). Under reducing conditions (β-mercaptoethanol), all constructs run as monomers (arrow 2 on the right gel). Cyt, cytoplasm; Ex, extracellular. Uncropped images for **e** are available as source data.

The oligomeric states of CALHMs are also the major determinants for pore diameters. We measured the pore diameter of CALHM1 as approximately 19.5 Å, which is similar to the previously reported diameter, 14 Å, estimated on the basis of a dye-permeation assay[15]. In our CALHM1 structure, the extra cryo-EM density extending from Ile 22 does not account for the remainder


a

b

c

d

e
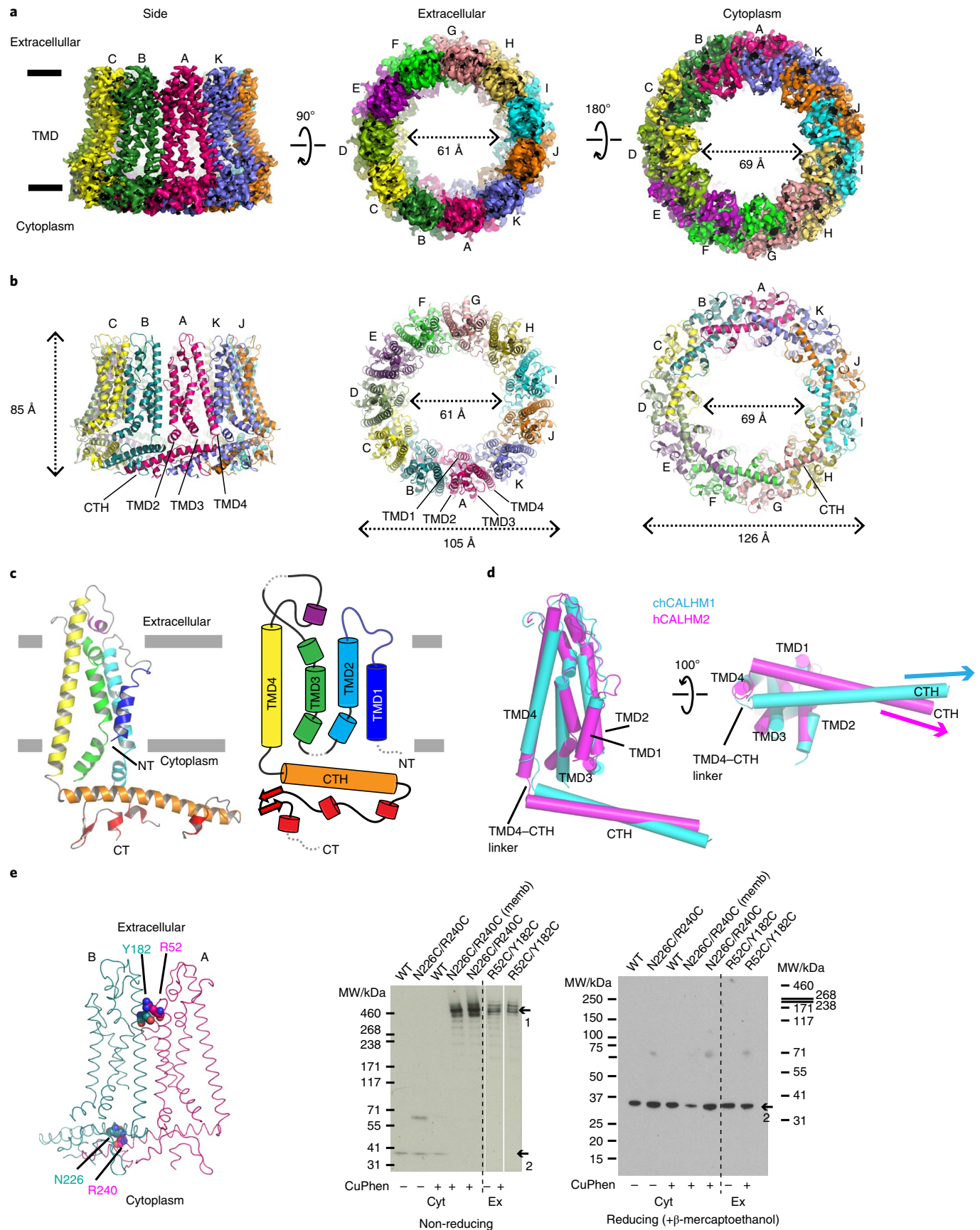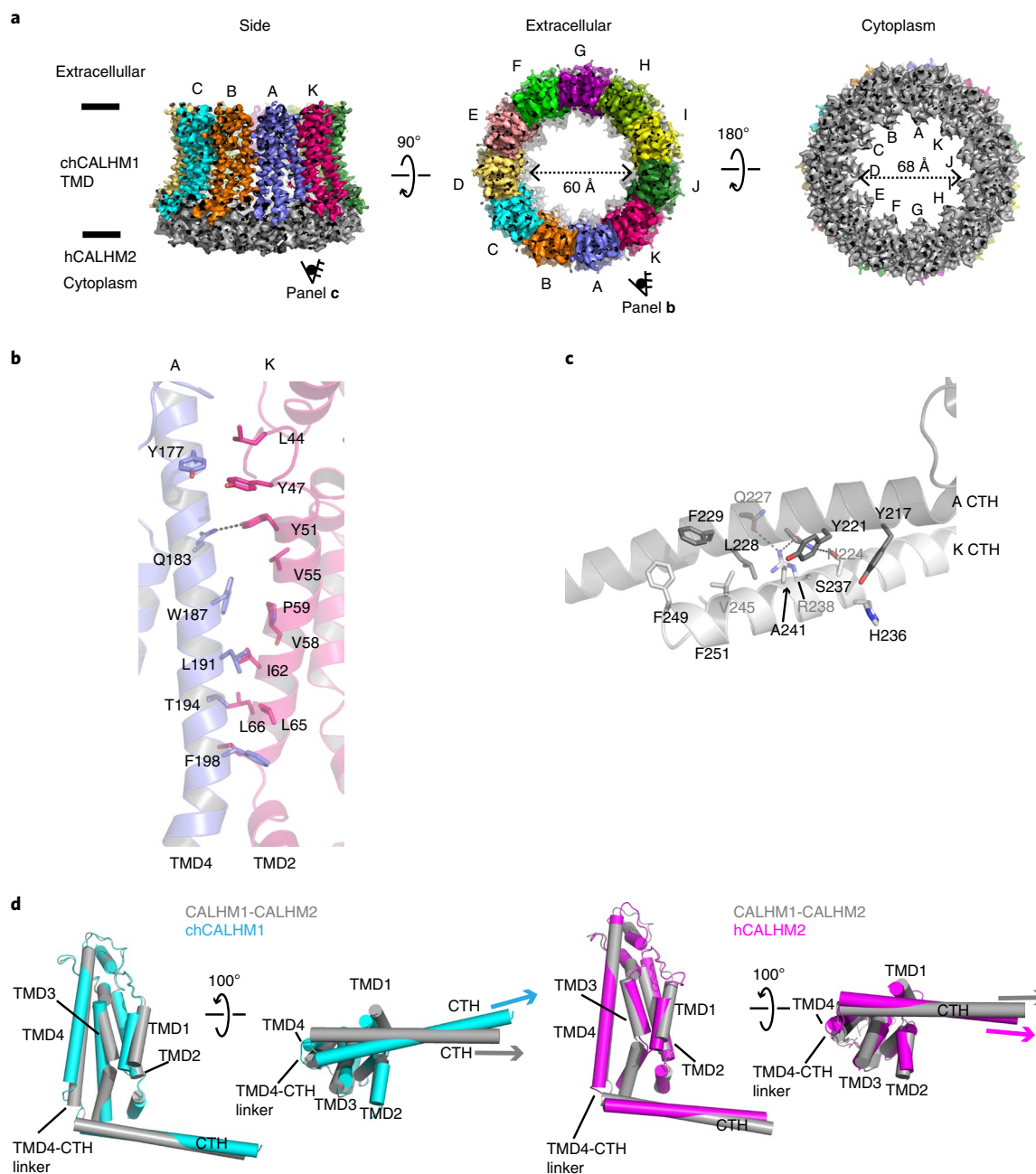
Fig. 4 | Structure of the CALHM1–CALHM2 chimera. a, Cryo-EM density of CALHM1–CALHM2 chimera viewed from the side of the TMDs, the extracellular region and the cytoplasm. The TMDs of each subunit are colored differently and the cytoplasmic domains are in gray. CALHM1–CALHM2 assembles as an undecamer similar to hCALHM2. **b,c**, The intersubunit interactions between TMD2 and TMD4 (**b**) and between CTHs (**c**). **d**, Comparison of protomers of the CALHM1–CALHM2 (gray), chCALHM1 (cyan) and hCALHM2 (magenta) demonstrating the similar and distinct TMD4–CTH orientations between CALHM1–CALHM2 and hCALHM2 and between CALHM1–CALHM2 and chCALHM1, respectively.

of the amino-terminal residues; thus, the actual pore diameter may be slightly smaller than 19.5 Å. Nevertheless, one of the important functions of CALHM1 is its capability to allow permeation of ATP, and the pore size observed here is well suited to mediate this. The undecamer assembly of CALHM2 results in a much greater pore diameter (~60 Å) compared to that of CALHM1, and a weak and amorphous cryo-EM density discontinuous from the CALHM2 proteins was observed in the middle of the channel. While some of the density may be derived from the amino-terminal residues, it is possible that hydrophobic compounds such as lipids exist in the middle of the channel, since the channel-lining residues of the TMD1 helices are hydrophobic in CALHM2 and are not favored to

becoming exposed to solvent. Such a presence of hydrophobic compounds may account for a lack of voltage-gated ion conductance in CALHM2, as reported previously[8] and as we have confirmed in this study (Fig. 1a). The existence of lipids in an oligomeric membrane protein assembly was previously observed in the structure of the bacteriorhodopsin trimers in 2D crystals[27]. These lipids likely strengthen the trimeric assembly and also prevent ions and metabolites from permeating through the oligomeric center.

In conclusion, our study demonstrates that CAHLM1 and CALHM2 assemble as octamers and undecamers, respectively, and that these different oligomeric states of CALHMs correlate with channel functions, with only the smaller octamer assembly displaying
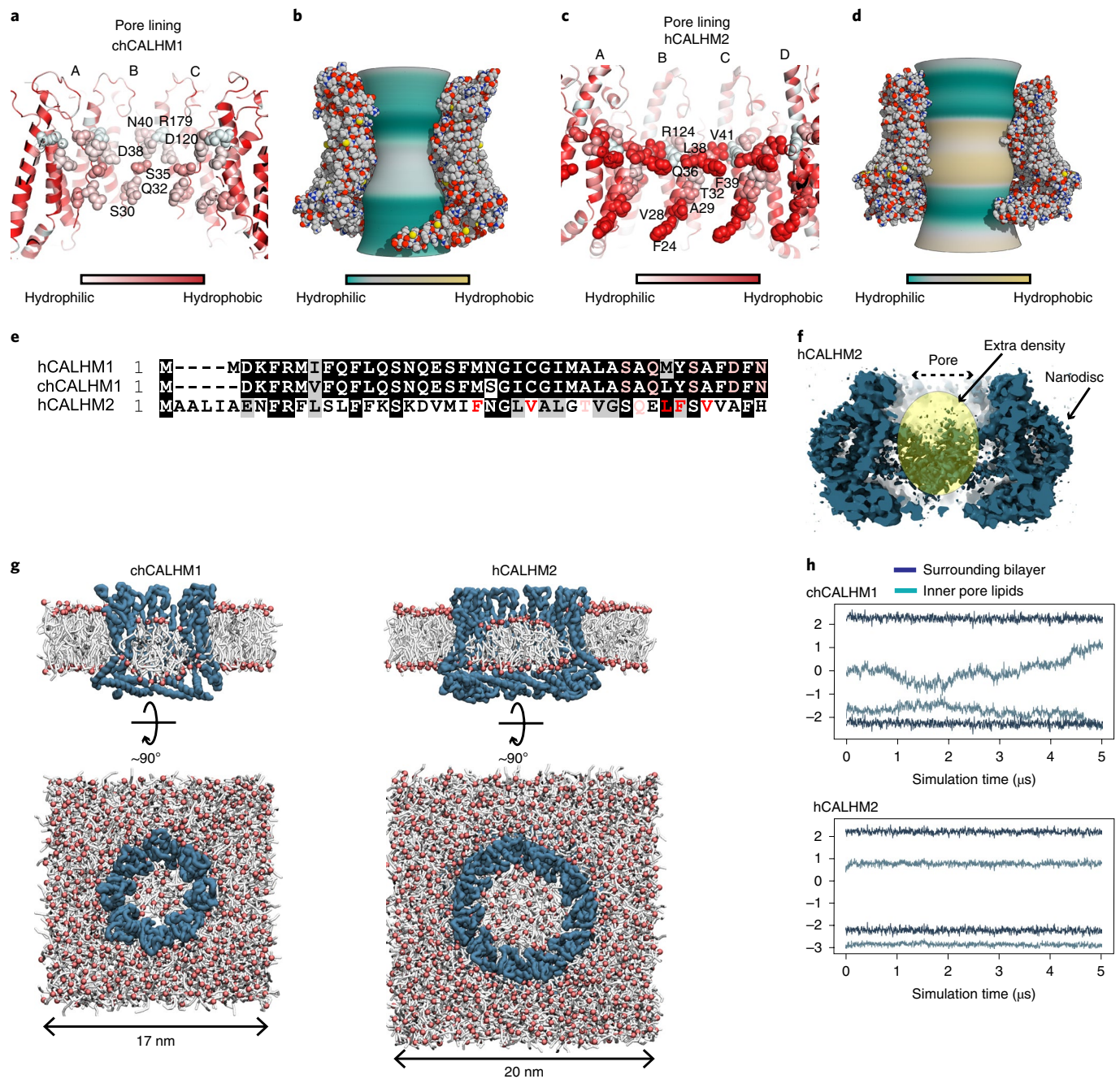
Fig. 5 | Comparison of pore properties between chCALHM1 and hCALHM2. a–d, Channel-lining residues (**a** and **c**)[28] and inner pore surface (**b** and **d**; calculated by CHAP[29]) of chCALHM1 (**a,b**) and hCALHM2 (**c,d**) colored on the basis of relative hydrophobicity. These parameters are calculated on the basis of the modeled residues; thus, the amino-terminal ends are not taken into account. **e**, Sequence alignment of the amino-terminal residues showing hydrophobic and hydrophilic residues facing the pore, with the same color code as in **a** and **c**. **f**, Cross-section of the hCALHM2 showing extra cryo-EM density in the middle of the pore. **g**, Coarse-grained molecular dynamics simulations of chCALHM1 (left) and hCALHM2 (right) embedded in POPC membranes. Side (cutaway) and top views of the final frame of one 5-μs replicate are shown in each case, with the protein backbone particles in blue, phospholipid headgroups in red and acyl tails in white. Water and ions present in the simulation systems are omitted for clarity. **h**, Headgroup positions of lipids inside each channel pore and in the surrounding bilayer membrane. The average headgroup z coordinates of lipids constituting the upper and lower leaflets in the final frame of each simulation are respectively tracked through the 5-μs simulated duration; results from one replicate are shown for each protein.

ion-channel activity. The structural information presented here will serve as a foundation to study mechanistic questions and for the development of reagents for CALHMs.

Online content

Any methods, additional references, Nature Research reporting summaries, source data, extended data, supplementary information,

acknowledgements, peer review information; details of author contributions and competing interests; and statements of data and code availability are available at https://doi.org/10.1038/s41594-019-0369-9.

References

1. Jun, M. et al. Calhm2 governs astrocytic ATP releasing in the development of depression-like behaviors. *Mol. Psychiatry* **23**, 883–891 (2018).
2. Vingtdeux, V. et al. CALHM1 deficiency impairs cerebral neuron activity and memory flexibility in mice. *Sci. Rep.* **6**, 24250 (2016).
3. Dreses-Werringloer, U. et al. A polymorphism in CALHM1 influences Ca^{2+} homeostasis, Aβ levels, and Alzheimer's disease risk. *Cell* **133**, 1149–1161 (2008).
4. Taruno, A. et al. CALHM1 ion channel mediates purinergic neurotransmission of sweet, bitter and umami tastes. *Nature* **495**, 223–226 (2013).
5. Ma, Z. et al. Calcium homeostasis modulator 1 (CALHM1) is the pore-forming subunit of an ion channel that mediates extracellular Ca^{2+} regulation of neuronal excitability. *Proc. Natl Acad. Sci. USA* **109**, E1963–E1971 (2012).
6. Vingtdeux, V. et al. Effect of the CALHM1 G330D and R154H human variants on the control of cytosolic Ca^{2+} and Aβ levels. *PLoS One* **9**, e112484 (2014).
7. Workman, A. D. et al. CALHM1-mediated ATP release and ciliary beat frequency modulation in nasal epithelial cells. *Sci. Rep.* **7**, 6687 (2017).
8. Ma, Z. et al. CALHM3 is essential for rapid ion channel-mediated purinergic neurotransmission of GPCR-mediated tastes. *Neuron* **98**, 547–561.e10 (2018).
9. Tanis, J. E. et al. CLHM-1 is a functionally conserved and conditionally toxic Ca^{2+}-permeable ion channel in *Caenorhabditis elegans*. *J. Neurosci.* **33**, 12275–12286 (2013).
10. Kawate, T. & Gouaux, E. Fluorescence-detection size-exclusion chromatography for precrystallization screening of integral membrane proteins. *Structure* **14**, 673–681 (2006).
11. Regan, M. C. et al. Structural mechanism of functional modulation by gene splicing in NMDA receptors. *Neuron* **98**, 521–529.e3 (2018).
12. Harauz, G. & van Heel, M. Exact filters for general geometry three dimensional reconstruction. *Optik* **73**, 146–156 (1986).
13. Rosenthal, P. B. & Henderson, R. Optimal determination of particle orientation, absolute hand, and contrast loss in single-particle electron cryomicroscopy. *J. Mol. Biol.* **333**, 721–745 (2003).
14. Slabinski, L. et al. XtalPred: a web server for prediction of protein crystallizability. *Bioinformatics* **23**, 3403–3405 (2007).
15. Siebert, A. P. et al. Structural and functional similarities of calcium homeostasis modulator 1 (CALHM1) ion channel with connexins, pannexins, and innexins. *J. Biol. Chem.* **288**, 6140–6153 (2013).
16. Tanis, J. E., Ma, Z. M. & Foskett, J. K. The NH_2 terminus regulates voltage-dependent gating of CALHM ion channels. *Am. J. Physiol. Cell Physiol.* **313**, C173–C186 (2017).
17. Oshima, A. et al. Atomic structure of the innexin-6 gap junction channel determined by cryo-EM. *Nat. Commun.* **7**, 13681 (2016).
18. Karakas, E. & Furukawa, H. Crystal structure of a heterotetrameric NMDA receptor ion channel. *Science* **344**, 992–997 (2014).
19. Lee, C. H. et al. NMDA receptor structures reveal subunit arrangement and pore architecture. *Nature* **511**, 191–197 (2014).
20. Maeda, S. et al. Structure of the connexin 26 gap junction channel at 3.5 Å resolution. *Nature* **458**, 597–602 (2009).
21. Deneka, D., Sawicka, M., Lam, A. K. M., Paulino, C. & Dutzler, R. Structure of a volume-regulated anion channel of the LRRC8 family. *Nature* **558**, 254–259 (2018).
22. Kasuya, G. et al. Cryo-EM structures of the human volume-regulated anion channel LRRC8. *Nat. Struct. Mol. Biol.* **25**, 797–804 (2018).
23. Vingtdeux, V. et al. CALHM1 ion channel elicits amyloid-beta clearance by insulin-degrading enzyme in cell lines and in vivo in the mouse brain. *J. Cell Sci.* **128**, 2330–2338 (2015).
24. de Jong, D. H. et al. Improved parameters for the Martini coarse-grained protein force field. *J. Chem. Theory Comput.* **9**, 687–697 (2013).
25. Stansfeld, P. J. et al. MemProtMD: automated insertion of membrane protein structures into explicit lipid membranes. *Structure* **23**, 1350–1361 (2015).
26. Bhattacharyya, M. et al. Molecular mechanism of activation-triggered subunit exchange in Ca^{2+}/calmodulin-dependent protein kinase II. *Elife* **5**, e13405 (2016).
27. Grigorieff, N., Ceska, T. A., Downing, K. H., Baldwin, J. M. & Henderson, R. Electron-crystallographic refinement of the structure of bacteriorhodopsin. *J. Mol. Biol.* **259**, 393–421 (1996).
28. Eisenberg, D., Schwarz, E., Komaromy, M. & Wall, R. Analysis of membrane and surface protein sequences with the hydrophobic moment plot. *J. Mol. Biol.* **179**, 125–142 (1984).
29. Klesse, G., Rao, S., Sansom, M. S. P. & Tucker, S. J. CHAP: a versatile tool for the structural and functional annotation of ion channel pores. *J. Mol. Biol.* **431**, 3353–3365 (2019).

Methods

Cell lines. HEK293 (ATCC, catalog no. CRL-1573) are adherent cells. *Spodoptera frugiperda* (*Sf*9) cells (ThermoFisher) are suspension cells. Cell lines were not authenticated or tested for mycoplasma contamination.

Expression, purification and nanodisc reconstitution of CALHM1 and CALHM2. The chCALHM1 or CALHM1-2 construct with amino-terminally fused Strep-II, 8×His tag, EGFP and the 3C protease site (StrepII2-His8-GFP) and the hCALHM2 construct with a carboxy-terminally fused Strep-II tag were expressed in the baculovirus (BV)/*Sf*9 system under the *Drosophila* Hsp70 promoter as previously described[11]. In brief, *Sf*9 cells were cultured in CCM3 (Invitrogen) supplemented with 1% nonheat-inactivated FBS at 27 °C, infected with BV at a cell density of 4×10^6 cells per ml and collected 48–52 h after infection. The collected cell pellets were resuspended in 20 mM HEPES–NaOH (pH 7.5), 200 mM NaCl, 1 mM EDTA and 1 mM PMSF and lysed under high-pressure homogenization (Avestin). The lysate was spun at 4,550*g* for 20 min and the supernatant was ultracentrifuged at 186,000*g* for 1 h at 4 °C. The pellet was solubilized in 20 mM HEPES–NaOH pH 7.5, 200 mM NaCl, 1 mM EDTA and 1% C12E8 (Anatrace) for 2 h at 4 °C and ultracentrifuged at 186,000*g* for 1 h at 4 °C. The clarified supernatant was loaded onto a Strep–Tactin Sepharose column followed by 20 column volumes of washing with 20 mM HEPES–NaOH (pH 7.5), 200 mM NaCl, 1 mM EDTA, 0.01% C12E8 (wash buffer) and elution using the wash buffer supplemented with 3 mM desthiobiotin. The purified hCALHM2 was concentrated to ~2.5 mg ml^{-1} at 4 °C using 100-kDa MWCO Amicon concentrators (Millipore) before reconstitution into nanodiscs. Purified chCALHM1 or CALHM1-2 was concentrated to 1 mg ml^{-1}, digested by trypsin at a weight-to-weight ratio of 1:20 for 1 h at 18 °C to remove StrepII2-His8-GFP and purified further by size-exclusion chromatography using a Superose 6 10/300 column (GE Healthcare) in 20 mM HEPES–NaOH (pH 7.5), 200 mM NaCl, 1 mM EDTA, 0.01% C12E8. Peak fractions were pooled and concentrated before reconstitution into nanodiscs. For reconstitution into nanodiscs, soybean polar extract, MSP2N2 and the purified CALHM proteins, at final concentrations of 0.75, 0.3 and 0.3 mg ml^{-1}, respectively, were mixed for 1 h at 4 °C, followed by detergent removal by SM2 Bio-Beads (BioRad) overnight (~12 h). The beads were removed and the solution was further purified by size-exclusion chromatography using a Superose 6 10/300 column (GE Healthcare) in 20 mM HEPES-NaOH pH 7.5, 200 mM NaCl, 1 mM EDTA. Peak fractions were pooled and concentrated to ~2.5 mg ml^{-1} (hCALHM2) or ~0.6 mg ml^{-1} (chCALHM1) for cryo-EM grid preparation. MSP2N2 protein was expressed and purified as previously described[30].

Cryo-EM sample preparation, image collection and single-particle analysis. The CALHM–nanodisc complex (3–4 µl) was applied to glow-discharged 1.2/1.3 400 mesh C-flat carbon-coated copper grids (Protochips). The grids were blotted for 4 s with blot force 7 at 85% humidity and 15 °C before plunge freezing into liquid ethane using a Vitrobot Mark IV (ThermoFisher). Here, it was critical to use blotting paper that was prewashed with 1 mM EDTA and dried to remove contaminations such as divalent cations. Usage of unwashed paper resulted in gap junction formation. Datasets were collected using a Titan Krios operated at an acceleration voltage of 300 keV and the GATAN K2 Summit direct electron detector coupled with the GIF quantum energy filter (Gatan) controlled by SerialEM software[31]. Movies were recorded with a pixel size of 1.06 Å, an exposure time of 10 s over 50 frames and a dose rate of 1.4 e$^-$ per Å^2 per frame. For chCALHM1, hCALHM2 and CALHM1-2, the program Warp was used to align movies, estimate the CTF and pick particles[32]. Two-dimensional classification, ab initio 3D map generation, 3D refinement, 3D classification, per-particle CTF refinement and *B* factor sharpening were performed using the program *cis*TEM[33]. For hCALHM2 gap junction, movie alignment and CTF estimation were carried out using the program Unblur[34] and CTFFind4 (ref.[35]), respectively, within the *cis*TEM package. Particle picking and the rest of the procedures were performed using *cis*TEM. The highest resolution of 3D refinement used was 6 Å for all of the models in this study. The workflows of single-particle analyses for chCALHM1, hCALHM2 and hCALHM2 gap junction are outlined in Extended Data Figs. 2, 5, 8 and 9. De novo modeling was done manually using the program Coot[36]. The final models were refined against the cryo-EM maps using PHENIX real-space refinement[37] with secondary structure and Ramachandran restraints. The FSCs were calculated by phenix.mtriage. Data collection and refinement statistics are summarized in Table 1. Local resolutions were estimated using the program ResMap[38].

Cysteine cross-linking and western blot analysis. The cysteine-substituted Asn226Cys/Arg240Cys hCALHM2 and Arg52Cys/Tyr182Cys hCALHM2, as well as wild-type hCALHM2, were all carboxy-terminally 1D4-tagged and expressed in the BV/*Sf*9 expression system under the cytomegalovirus promoter. The membrane fractions were isolated and solubilized as above. The solubilized fraction was subjected to affinity purification by 1D4 antibody conjugated to CNBr-activated agarose (GE Healthcare). The resin was extensively washed and the protein eluted with wash buffer supplemented with 0.2 mg ml^{-1} 1D4 peptide. Samples were then either reduced with β-mercaptoethanol, left untreated or treated with the oxidizing agent (1,10-phenanthroline) copper(ii). After 30 min

incubation on ice, 1 mM final concentration iodoacetamide was added to samples treated with (1,10-phenanthroline) copper(ii). Samples were subjected to western blot using monoclonal anti-1D4 (University of British Columbia) and anti-mouse horseradish peroxidase-conjugated (GE Healthcare). Protein bands were detected by enhanced chemiluminescence on X-ray film (ECL kit; GE Healthcare). To verify that the in-membrane hCALHM2 assembly corresponded in size to detergent-extracted hCALHM2, the membrane fractions containing Asn226Cys/Arg240Cys hCALHM2-1D4 were also oxidized with (1,10-phenanthroline) copper(ii) before solubilization with detergent.

Molecular dynamics. Molecular structures of chCALHM1 and hCALHM2 were separately embedded within POPC bilayer membranes that were solvated on either side at 0.2 M NaCl concentration. Simulation cells were of approximate dimensions $17 \times 17 \times 15$ nm^3 (CALHM1) and $20 \times 20 \times 15$ nm^3 (CALHM2). Each protein–membrane system was assembled and equilibrated via a previously established protocol[25]. Simulations were performed with GROMACS v.5.1 (ref.[39]). The Martini v.2.2 force field[24] was used for coarse-grained simulations, with a time step of 20 fs and an elastic network used to harmonically restrain Cα particles and stabilize the protein structure. Atomistic simulations were run using the OPLS all-atom protein force field with united-atom lipids[40] and the TIP4P/2005 water model[41]. The integration time step was 2 fs. Temperature and pressure were maintained at 37 °C and 1 bar during simulations using the velocity-rescaling thermostat[42] in combination with a semi-isotropic Parrinello and Rahman barostat[43], with coupling constants of $\tau_T = 0.1$ ps and $\tau_P = 1$ ps, respectively. Bonds were constrained through the LINCS algorithm[44]. A Verlet cut-off scheme was applied, and long-range electrostatic interactions were calculated using the particle mesh Ewald method[45].

Electrophysiology. CALHM proteins were expressed in HEK293T cells infected by the recombinant BV harboring chCALHM1 or hCALHM under the cytomegalovirus promoter. Recordings were obtained ~48 h postinfection using borosilicate glass pipettes (Sutter Instruments) pulled and polished to a final resistance of 2–6 MΩ and backfilled with 147 mM NaCl, 10 mM EGTA and 10 mM HEPES pH 7.0 with NaOH. The bath solution contained 147 mM NaCl, 13 mM glucose, 10 mM HEPES pH 7.3 with NaOH, 2 mM KCl, 2 mM CaCl$_2$ and 1 mM MgCl$_2$. Recordings performed in the absence of Ca^{2+} used a similar solution but with no CaCl$_2$ added. A rapid solution exchanger (RSC-200; Bio-logic) was used to perfuse cells with various solutions. All of the recordings were done at 22 °C. Data were collected on an AxoPatch 200B patch-clamp amplifier (Axon Instruments), filtered at 2 kHz (Frequency Devices) and digitized with a Digidata 1550B digitizer (Axon Instruments) using a sampling frequency of 10 kHz. Recordings were analyzed using the Clampex 11.0 software (Axon Instruments). Patches were held at −60 mV and stepped between −100 mV and +100 mV in 20-mV increments for 1 s.

Reporting Summary. Further information on research design is available in the Nature Research Reporting Summary linked to this article.

Data availability

Cryo-EM maps and structural coordinates generated during this study have been deposited in the Electron Microscopy Data Bank and Protein Data Bank with accession codes: EMD-21143 and PDB 6VAM (chCALHM1), EMD-21141 and PDB 6VAK (hCALHM2), EMD-21140 and PDB 6VAI (hCALHM2 gap junction) and EMD-21142 and PDB 6VAL (chCALHM1–hCALHM2 chimera). Source data for Figs. 1b and 3e are available with the paper online.

References

30. Ritchie, T. K. et al. Reconstitution of membrane proteins in phospholipid bilayer nanodiscs. *Methods Enzymol.* **464**, 211–231 (2009).
31. Schorb, M., Haberbosch, I., Hagen, W. J. H., Schwab, Y. & Mastronarde, D. N. Software tools for automated transmission electron microscopy. *Nat. Methods* **16**, 471–477 (2019).
32. Tegunov, D. & Cramer, P. Real-time cryo-electron microscopy data preprocessing with Warp. *Nat. Methods* **16**, 1146–1152 (2019).
33. Grant, T., Rohou, A. & Grigorieff, N. *cis*TEM, user-friendly software for single-particle image processing. *Elife* **7**, e35383 (2018).
34. Grant, T. & Grigorieff, N. Measuring the optimal exposure for single particle cryo-EM using a 2.6 Å reconstruction of rotavirus VP6. *Elife* **4**, e06980 (2015).
35. Rohou, A. & Grigorieff, N. CTFFIND4: fast and accurate defocus estimation from electron micrographs. *J. Struct. Biol.* **192**, 216–221 (2015).
36. Emsley, P., Lohkamp, B., Scott, W. G. & Cowtan, K. Features and development of Coot. *Acta Crystallogr. D Biol. Crystallogr.* **66**, 486–501 (2010).
37. Adams, P. D. et al. PHENIX: a comprehensive Python-based system for macromolecular structure solution. *Acta Crystallogr. D Biol. Crystallogr.* **66**, 213–221 (2010).
38. Kucukelbir, A., Sigworth, F. J. & Tagare, H. D. Quantifying the local resolution of cryo-EM density maps. *Nat. Methods* **11**, 63–65 (2014).

39. Abraham, M. J. et al. GROMACS: high performance molecular simulations through multi-level parallelism from laptops to supercomputers. *SoftwareX* **1–2**, 19–25 (2015).

40. Jorgensen, W. L., Maxwell, D. S. & Tirado-Rives, J. Development and testing of the OPLS all-atom force field on conformational energetics and properties of organic liquids. *J. Am. Chem. Soc.* **118**, 11225–11236 (1996).

41. Abascal, J. L. F. & Vega, C. A general purpose model for the condensed phases of water: TIP4P/2005. *J. Chem. Phys.* **123**, 234505 (2005).

42. Bussi, G., Donadio, D. & Parrinello, M. Canonical sampling through velocity rescaling. *J. Chem. Phys.* **126**, 014101 (2007).

43. Parrinello, M. & Rahman, A. Polymorphic transitions in single crystals: a new molecular dynamics method. *J. Appl. Phys.* **52**, 7182–7190 (1981).

44. Hess, B., Bekker, H., Berendsen, H. J. C. & Fraaije, J. G. E. M. LINCS: a linear constraint solver for molecular simulations. *J. Comput. Chem.* **18**, 1463–1472 (1997).

45. Darden, T., York, D. & Pedersen, L. Particle mesh Ewald: an $N \cdot \log(N)$ method for Ewald sums in large systems. *J. Chem. Phys.* **98**, 10089–10092 (1993).

Author contributions

J.L.S., T.-H.C., T.G., N.S., N.G. and H.F. designed and conducted experiments involving cryo-EM. K.M. conducted electrophysiology experiments. S.R. and S.J.T. conducted computational simulations. All authors wrote the manuscript.

Competing interests

The authors declare no competing interests.

Additional information

Extended data is available for this paper at https://doi.org/10.1038/s41594-019-0369-9.

Supplementary information is available for this paper at https://doi.org/10.1038/s41594-019-0369-9.

Correspondence and requests for materials should be addressed to H.F.

Peer review information Katarzyna Marcinkiewicz was the primary editor on this article and managed its editorial process and peer review in collaboration with the rest of the editorial team.

Reprints and permissions information is available at www.nature.com/reprints.
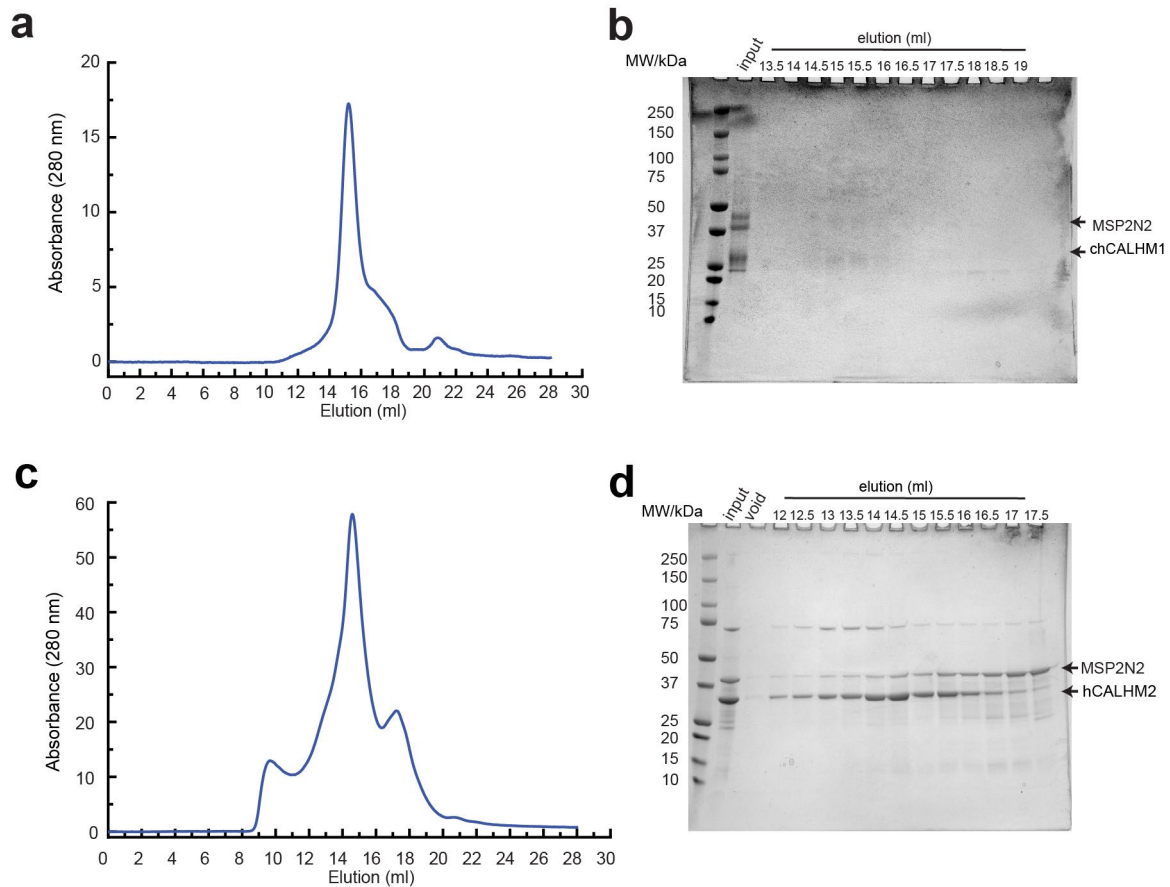
Extended Data Fig. 1 | Reconstitution of chCALHM1 and hCALHM2 into lipid nanodiscs. a, Representative Superose-6 SEC chromatograph of chCALHM1 in MSP2N2 nanodiscs with soy polar extract. **b**, SDS-PAGE of the fractions collected from SEC. The band for chCALHM1 has a tendency to spread out in SDS-PAGE. Fractions that eluted between 13.5-15.5 ml were pooled, concentrated and subjected to cryo-EM. **c**, Representative Superose 6 SEC chromatograph of hCALHM2 in MSP2N2 nanodiscs with soy polar extract. **d**, SDS-PAGE of the fractions collected from SEC. Fractions that eluted between 14.5-16.5 ml were pooled, concentrated and subjected to cryo-EM.
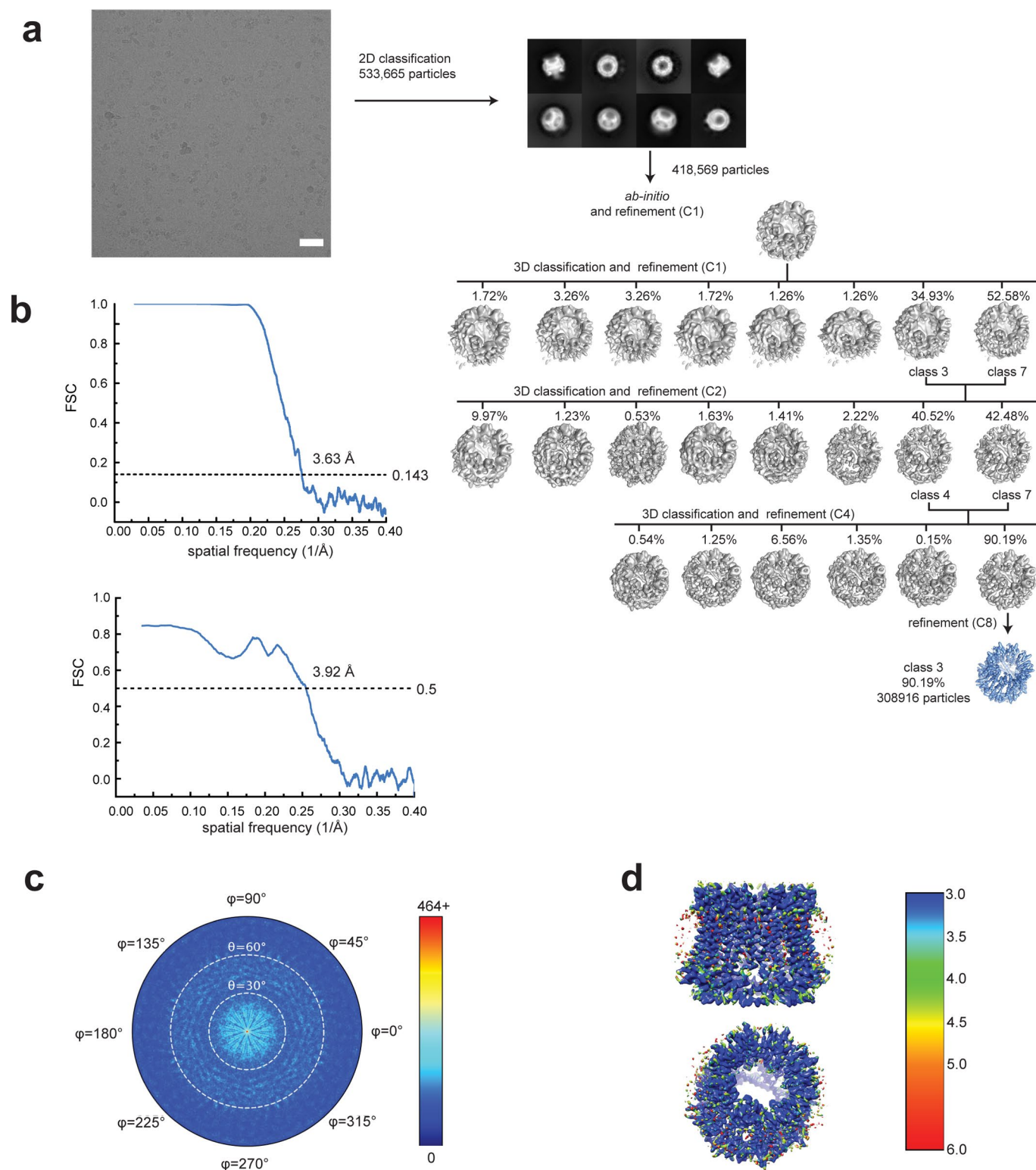
Extended Data Fig. 2 | Single particle analysis of chCALHM1. a, A representative micrograph (scale bar = 38.8 nm), representative 2D class averages, and the 3D classification workflow are shown. **b,** The FSC plots of the two half maps (top) and the map vs model (bottom) are shown. **c,** The angular distribution plot for class 3. **d,** Local resolutions of class 3 were calculated using ResMap.
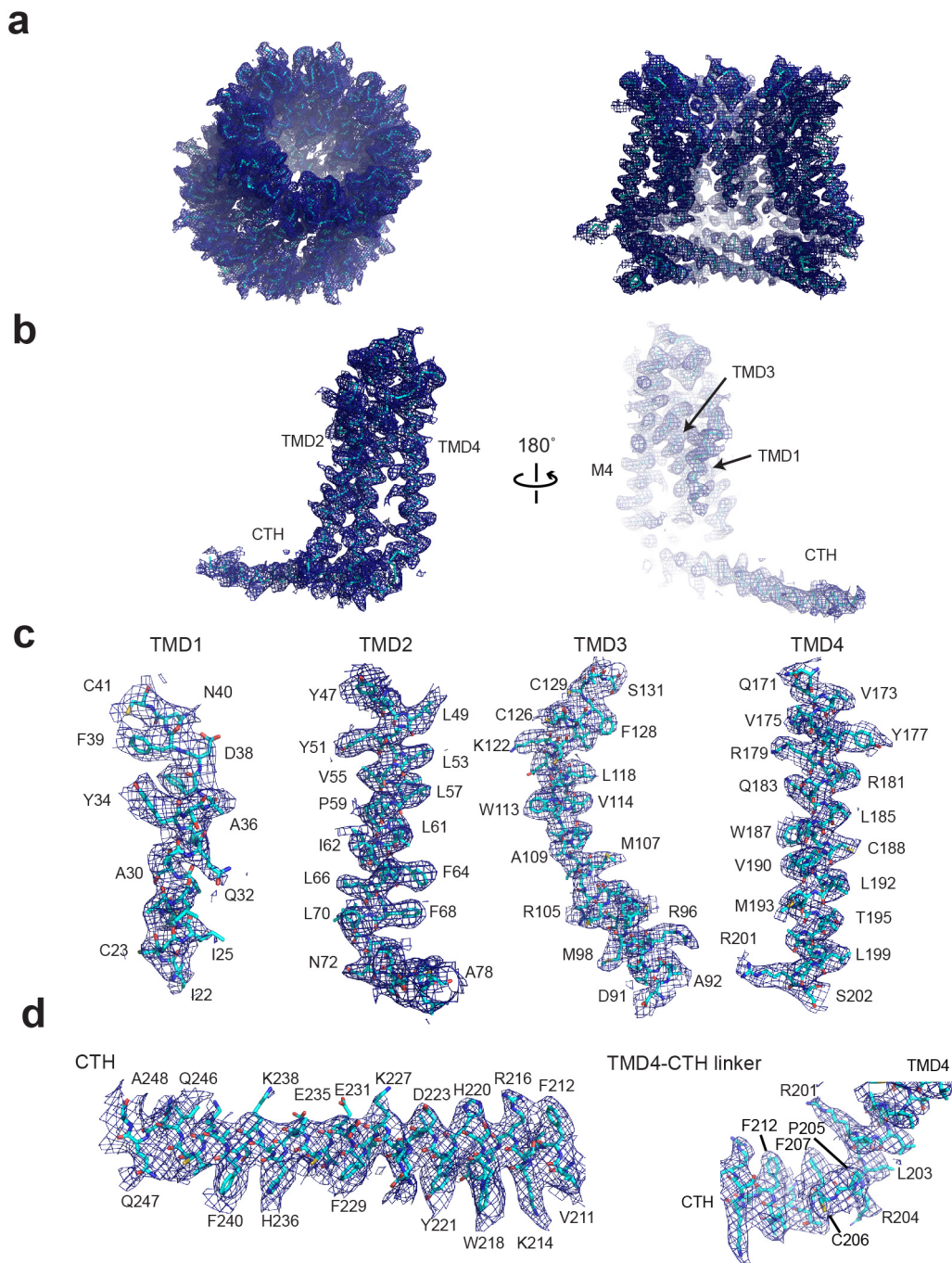
Extended Data Fig. 3 | Representative cryo-EM density of chCALHM1. a, Cryo-EM density of the overall octameric assembly (left) and the cross-sectional view of the central cavity (right). **b–c**, Representative density for a monomer (**b**), and individual TMDs (**c**), and a CTH and a TMD4-CTH linker.
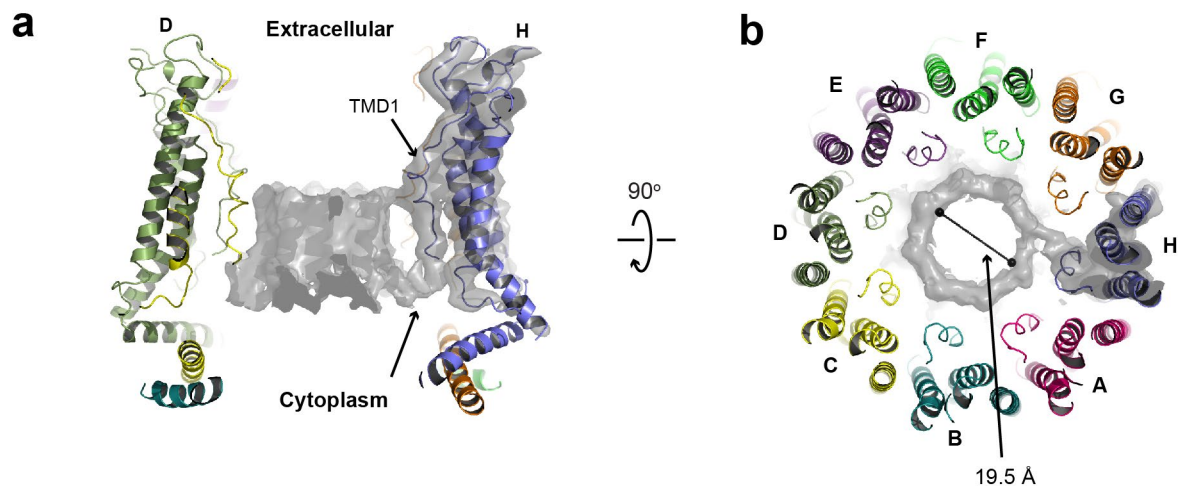
Extended Data Fig. 4 | Presence of extra cryo-EM density in the chCALHM1 pore. a, Extra cryo-EM density is observed in the middle of the pore-like structure of chCALHM1. Here, the pore-density and the density for only subunit H are shown for clarity. TMD1 and the pore-density are continuous (arrow). **b**, The density observed from the top of the extracellular region. The diameter of the pore is 19.5 Å.

Extended Data Fig. 5 | Single particle analysis of hCALHM2. a, A representative micrograph (scale bar = 38.8 nm), representative 2D class averages, and the 3D classification workflow are shown. **b**, The FSC plots of the two half maps (top) and the map vs. model (bottom) are shown for class 8. **c**, The angular distribution plot for class 8. **d**, Local resolutions of class 8 were calculated using ResMap.
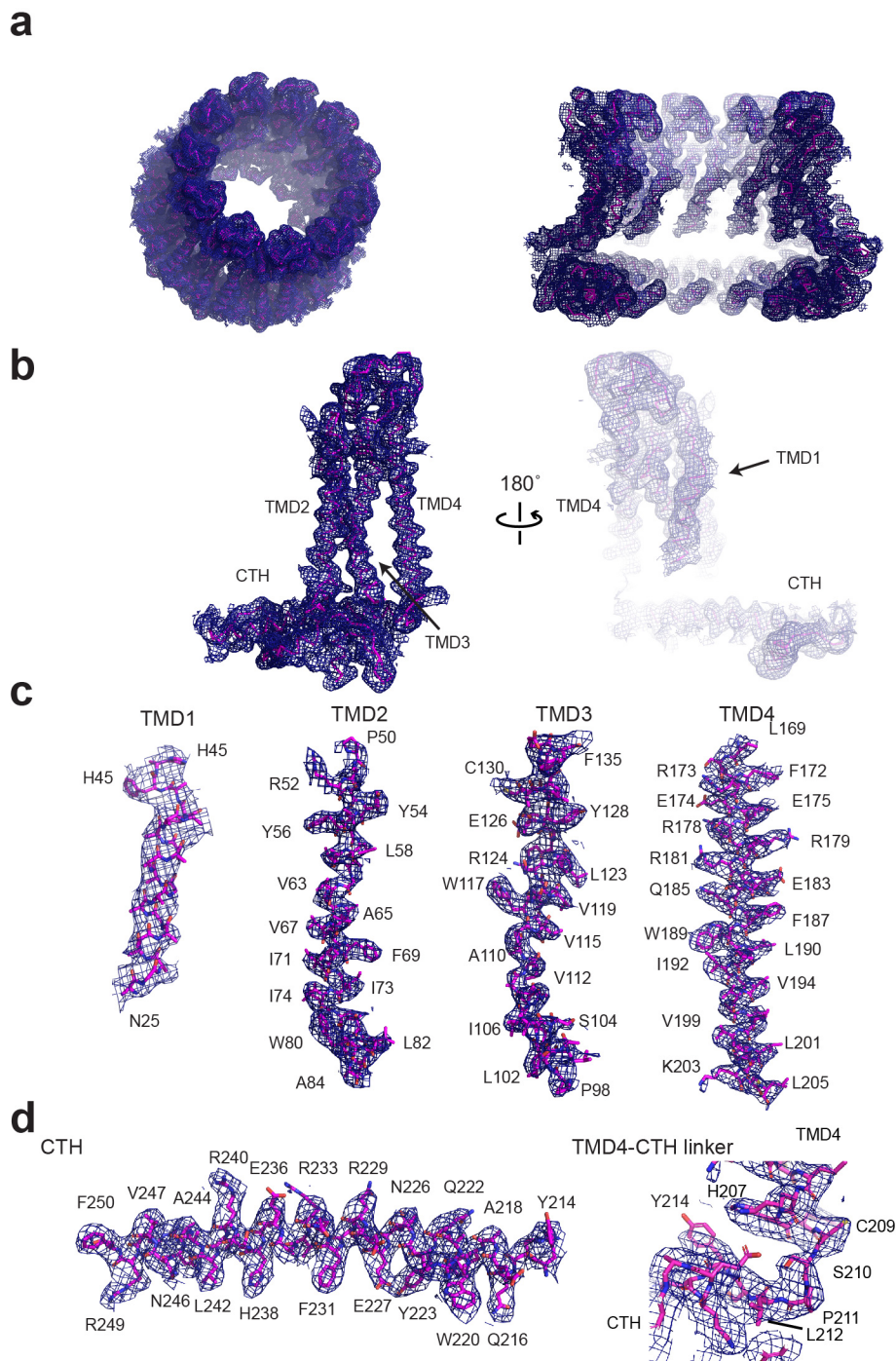
Extended Data Fig. 6 | Representative cryo-EM density of hCALHM2. a, Cryo-EM density of the overall 11-mer assembly (left) and the cross-sectional view of the central cavity (right). **b–c**, Representative density for a monomer (**b**), and individual TMDs (**c**) and a CTH and a TMD4-CTH linker.
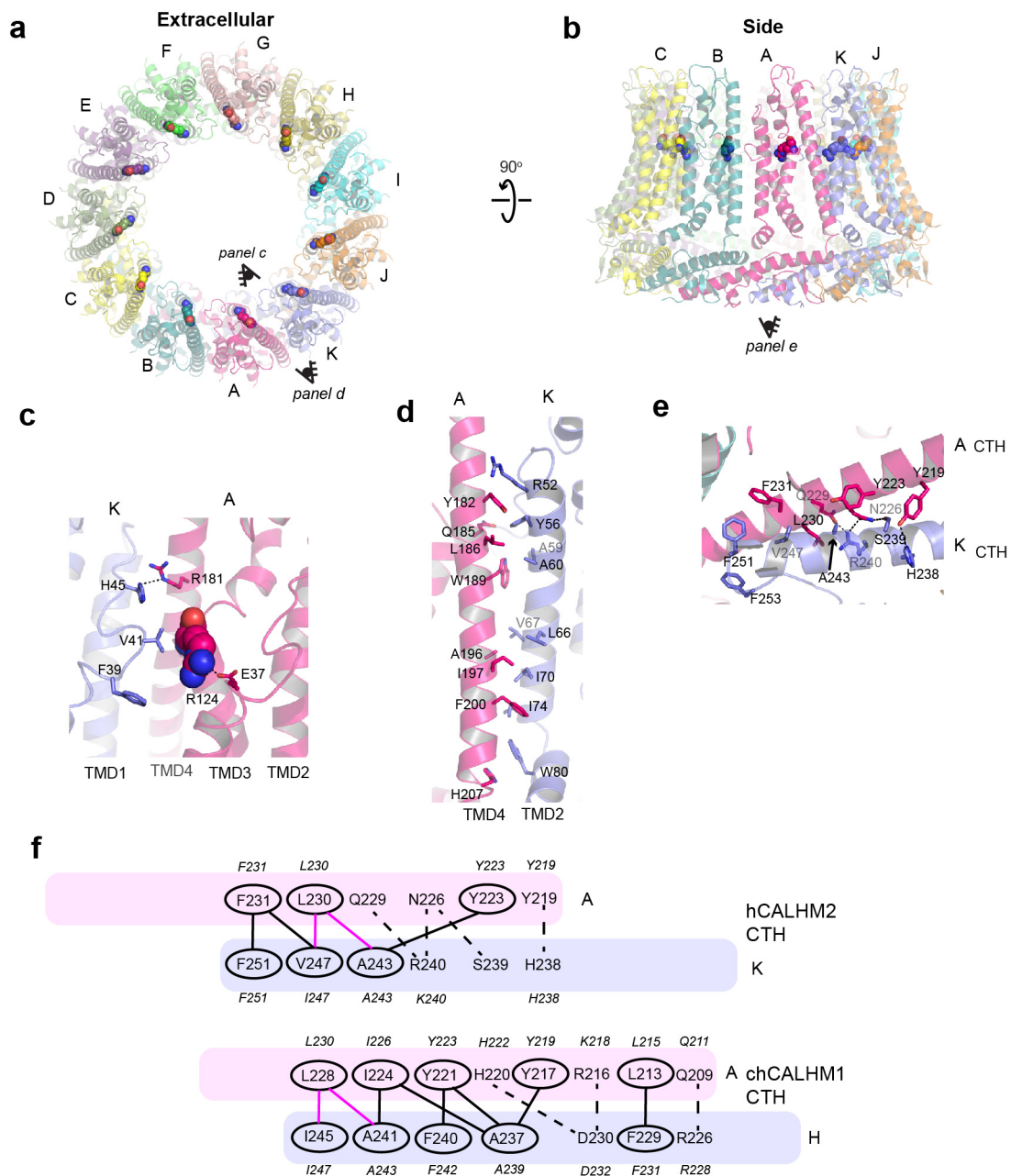
Extended Data Fig. 7 | Interaction of hCALHM2 subunits. a–b, The hCALHM2 structure viewed from the top of extracellular region (**a**) and the side of the membrane (**b**). Shown in spheres are the Arg124 residues at the equivalent position to chCALHM1 Asp120 or hCALHM1 Asp121. **c**, Arg124 (sphere) and surrounding residues (sticks) form polar and hydrophobic interactions to mediate inter-subunit interactions. **d–e**, The inter-subunit interactions between TMD2 and TMD4 (**d**) and CTHs (**e**). **f**, The schematic presentation of the interactions between two CTHs (magenta and slate blue) in hCALHM2 (top) and chCALHM1 (bottom). Polar and van der Waals interactions mediated by hydrophobic residues (ovals) are shown as dashed and solid lines, respectively. The lines in magenta are the conserved interactions between chCALHM1 and hCALHM2. The residues in italic are the equivalent ones in hCALHM1.
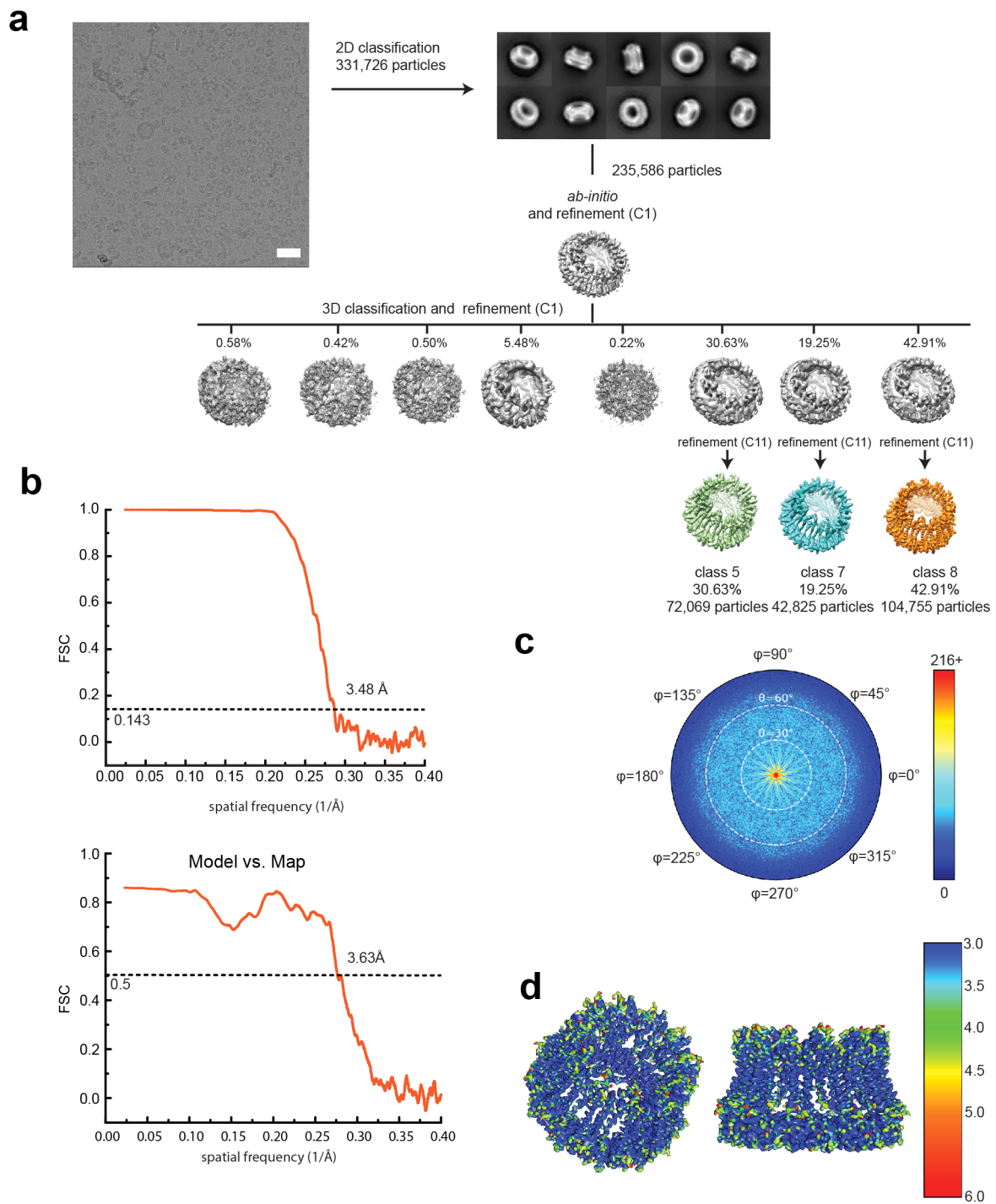
Extended Data Fig. 8 | Single particle analysis of CALHM1-2. a, A representative micrograph (scale bar = 40.5 nm), representative 2D class averages, and the 3D classification workflow are shown. **b**, The FSC plots of the two half maps (top) and the map vs. model (bottom) are shown for class 8. **c**, The angular distribution plot for class 8. **d**, Local resolutions of class 8 were calculated using ResMap.

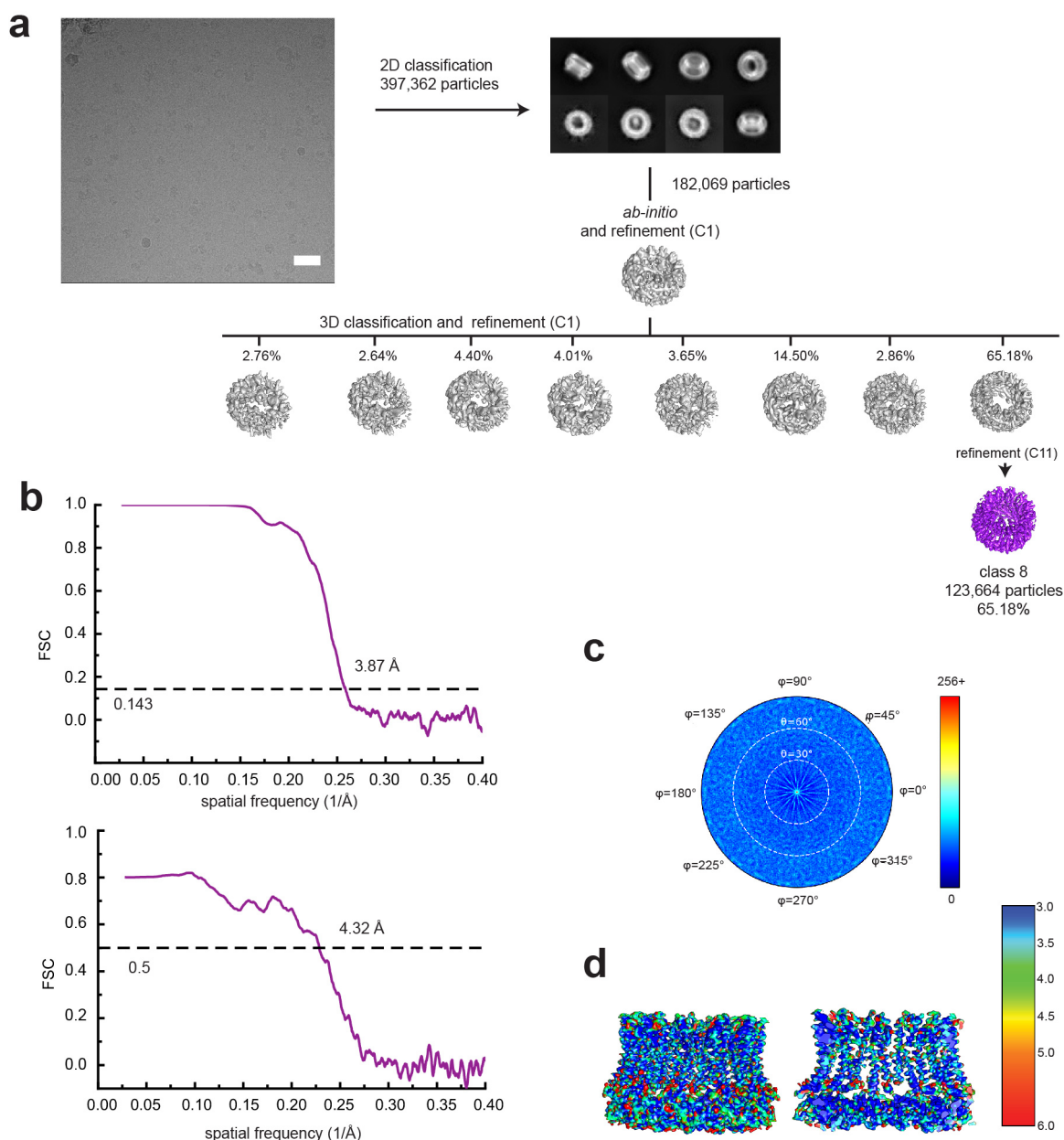**Extended Data Fig. 9 | Single particle analysis of 22-meric hCALHM2. a**, A representative micrograph (scale bar = 38.8 nm), representative 2D class averages, and the 3D classification workflow are shown. **b**, The FSC plots of the two half maps (top) and the map vs. model (bottom) are shown for class 8. **c**, The angular distribution plot for class 8. **d**, Local resolutions of class 8 were calculated using ResMap.
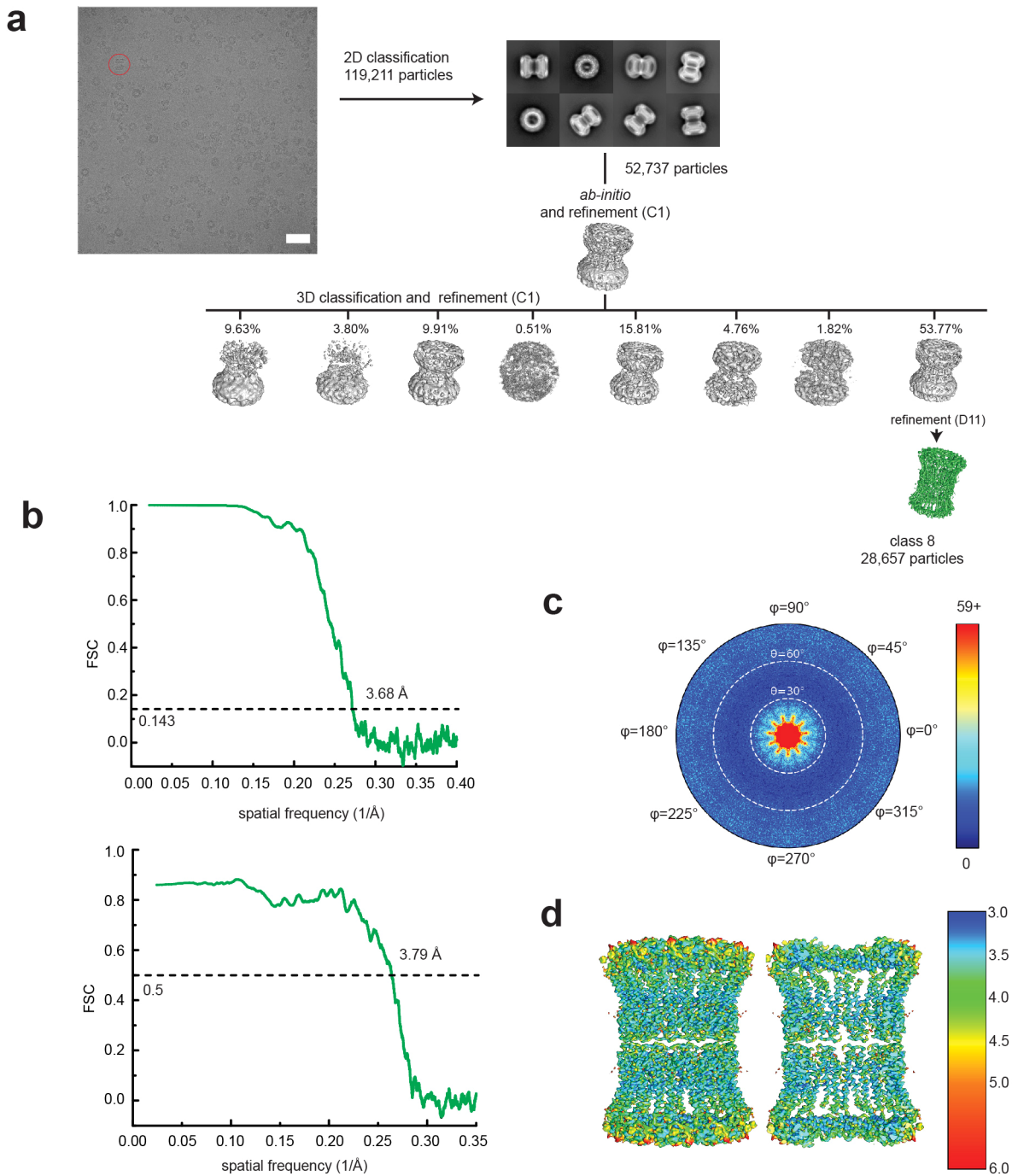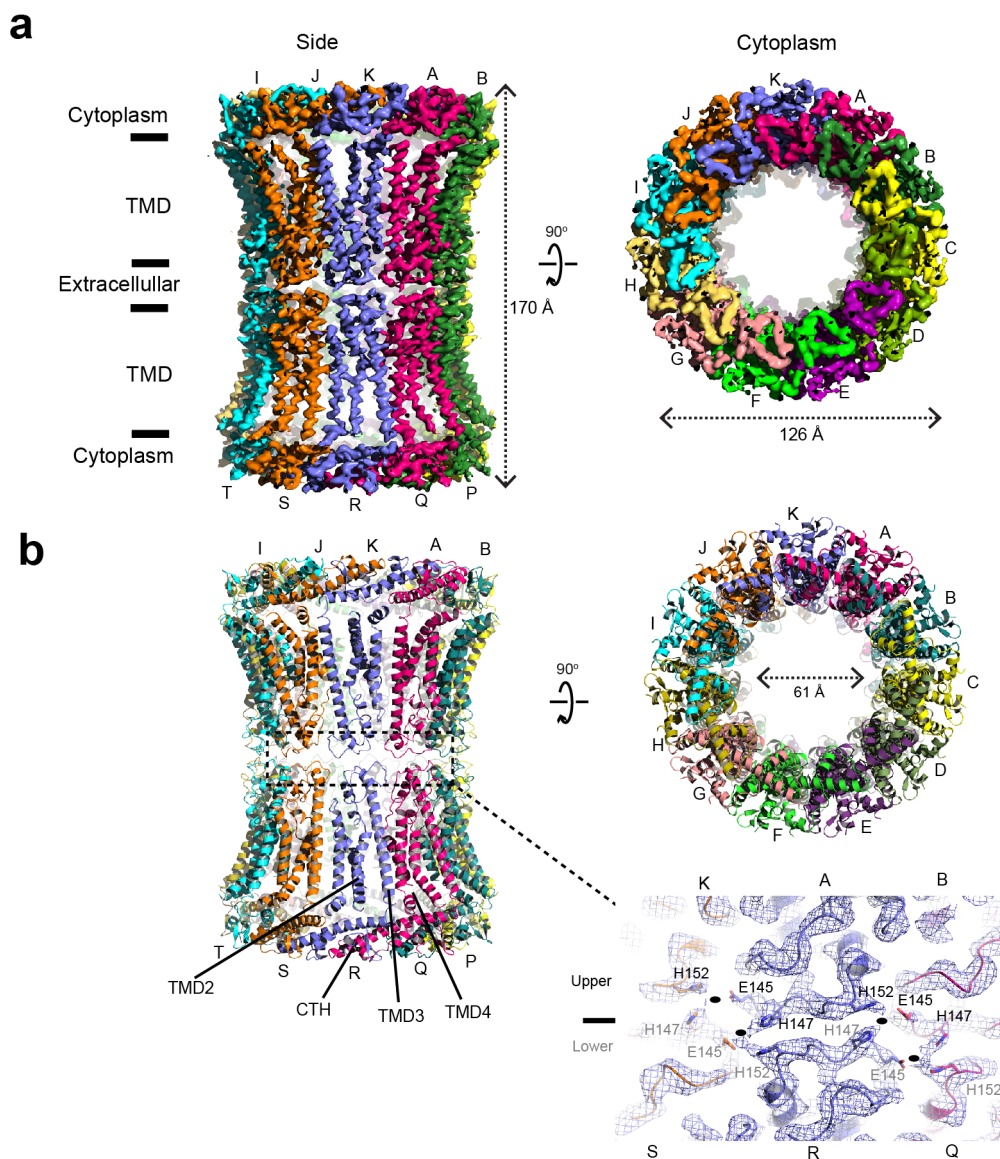
Extended Data Fig. 10 | Structure of hCALHM2 gap junction. a, Cryo-EM density of the 22-meric hCALHM2 viewed from the side of the membrane and from the cytoplasm. **b**, The structural models in the same orientation as the cryo-EM density in (**a**), showing locations of the TMD2-4 and the CTH. There is little or no structural change between the 22-mer and 11-mer structures except for the extracellular region (due to the inter-11-mer interaction). The interaction between the two hemichannels is mediated by His147, His152, and Glu145 in the extracellular loop between TMD3 and TMD4. Density between His147 and His152 is continuous implying the potential presence of a divalent cation. Residues from the upper and lower hemichannels are annotated with black and gray fonts. Ovals are placed at the interaction sites.

Corresponding author(s):   Hiro Furukawa

Last updated by author(s): Dec 17, 2019

Reporting Summary

Nature Research wishes to improve the reproducibility of the work that we publish. This form provides structure for consistency and transparency in reporting. For further information on Nature Research policies, see Authors & Referees and the Editorial Policy Checklist.

Statistics

For all statistical analyses, confirm that the following items are present in the figure legend, table legend, main text, or Methods section.

n/a	Confirmed	
☐	☒	The exact sample size (*n*) for each experimental group/condition, given as a discrete number and unit of measurement
☐	☒	A statement on whether measurements were taken from distinct samples or whether the same sample was measured repeatedly
☒	☐	The statistical test(s) used AND whether they are one- or two-sided *Only common tests should be described solely by name; describe more complex techniques in the Methods section.*
☒	☐	A description of all covariates tested
☒	☐	A description of any assumptions or corrections, such as tests of normality and adjustment for multiple comparisons
☒	☐	A full description of the statistical parameters including central tendency (e.g. means) or other basic estimates (e.g. regression coefficient) AND variation (e.g. standard deviation) or associated estimates of uncertainty (e.g. confidence intervals)
☒	☐	For null hypothesis testing, the test statistic (e.g. *F*, *t*, *r*) with confidence intervals, effect sizes, degrees of freedom and *P* value noted *Give P values as exact values whenever suitable.*
☒	☐	For Bayesian analysis, information on the choice of priors and Markov chain Monte Carlo settings
☒	☐	For hierarchical and complex designs, identification of the appropriate level for tests and full reporting of outcomes
☒	☐	Estimates of effect sizes (e.g. Cohen's *d*, Pearson's *r*), indicating how they were calculated

Our web collection on statistics for biologists contains articles on many of the points above.

Software and code

Policy information about availability of computer code

Data collection	SerialEM was used to collect all of the cryo-EM data. Clampex 11.0 software (Axon Instruments) was used for collecting patch-clamp electrophysiology data. Molecular dynamics simulation was conducted using GROMACS 5.1 and CHAP.
Data analysis	WARP and cisTEM were used for image processing, CTF estimation, and particle extraction. Single particle analysis including 2D classification, ab-initio 3D reconstruction, 3D refinement, 3D classification, and per particle CTF refinement were performed using cisTEM.

For manuscripts utilizing custom algorithms or software that are central to the research but not yet described in published literature, software must be made available to editors/reviewers. We strongly encourage code deposition in a community repository (e.g. GitHub). See the Nature Research guidelines for submitting code & software for further information.

Data

Policy information about availability of data

All manuscripts must include a data availability statement. This statement should provide the following information, where applicable:
- Accession codes, unique identifiers, or web links for publicly available datasets
- A list of figures that have associated raw data
- A description of any restrictions on data availability

Cryo-EM maps and structural coordinates generated during this study will be deposited in the Electron Microscopy Data Bank with accession codes: ###, ###, and ###. We will have the accession codes as soon as we complete the submission.

Field-specific reporting

Please select the one below that is the best fit for your research. If you are not sure, read the appropriate sections before making your selection.

☒ Life sciences ☐ Behavioural & social sciences ☐ Ecological, evolutionary & environmental sciences

For a reference copy of the document with all sections, see nature.com/documents/nr-reporting-summary-flat.pdf

Life sciences study design

All studies must disclose on these points even when the disclosure is negative.

Sample size	Cryo-EM images were collected until the resolution and 3D reconstruction converges.
Data exclusions	Some patch recordings were exclude when there are artifacts associated with sealing of membranes of HEK293 cells associated with health of cells.
Replication	Patch clamp electrophysiology recordings were done from at least six individual patches.
Randomization	N.A.
Blinding	N.A.

Reporting for specific materials, systems and methods

We require information from authors about some types of materials, experimental systems and methods used in many studies. Here, indicate whether each material, system or method listed is relevant to your study. If you are not sure if a list item applies to your research, read the appropriate section before selecting a response.

Materials & experimental systems

n/a	Involved in the study
☐	☒ Antibodies
☐	☒ Eukaryotic cell lines
☒	☐ Palaeontology
☒	☐ Animals and other organisms
☒	☐ Human research participants
☒	☐ Clinical data

Methods

n/a	Involved in the study
☒	☐ ChIP-seq
☒	☐ Flow cytometry
☒	☐ MRI-based neuroimaging

Antibodies

Antibodies used	1D4 antibodies
Validation	1D4 antibodies are validated by the manufacturer at the University of British Columbia. https://uilo.ubc.ca/rho-1d4-antibody

Eukaryotic cell lines

Policy information about cell lines

Cell line source(s)	HEK293, Sf9
Authentication	All of the cell-lines used at Cold Spring Harbor Laboratory (CSHL) are going through the "Cell Authentication Service" at University of Arizona.
Mycoplasma contamination	The above celllines are tested for potential contamination with micoplasm.
Commonly misidentified lines (See ICLAC register)	N.A.

In the format provided by the authors and unedited.

Structure and assembly of calcium homeostasis modulator proteins

Johanna L. Syrjanen[1], Kevin Michalski[1], Tsung-Han Chou [1], Timothy Grant[2], Shanlin Rao[3,4], Noriko Simorowski[1], Stephen J. Tucker [3], Nikolaus Grigorieff [2,5] and Hiro Furukawa [1]*

[1]WM Keck Structural Biology Laboratory, Cold Spring Harbor Laboratory, Cold Spring Harbor, NY, USA. [2]Janelia Research Campus, Howard Hughes Medical Institute, Ashburn, VA, USA. [3]Department of Biochemistry, University of Oxford, Oxford, UK. [4]Clarendon Laboratory, Department of Physics, University of Oxford, Oxford, UK. [5]RNA Therapeutics Institute, University of Massachusetts Medical School, Worcester, MA, USA. *e-mail: furukawa@cshl.edu

TMD1

```
                               1        10        20        30        40        50
                               .        .         .         .         .         .
Gallus gallus/1-342        1   ....MDKFRMVFQF.LQSNQESFMSGICGIMALASAQLYSAFDFNCPCLPRYNLAYGLGV
Homo sapiens/1-348         1   ...MMDKFRMIFQF.LQSNQESFMNGICGIMALASAQMYSAFDFNCPCLPGYNAAYSAGI
Caenorhabditis elegans/1-329 1 MTTSINSVVTVFQNVFTNHGSTLLNGILIATTVGGQSLVRKLTFSCPCAYPLNIYHSLVF
Danio rerio/1-346          1   ....MDKFRIMVQF.LQANQESFMNGICGIMALASAQMYSSFEFTCPCLPDYNYAYGIGI
```

TMD2   TMD3

```
                               60        70        80      ↓  90       100       110
                               .         .         .          .         .         .
Gallus gallus/1-342        56  LLVPPLILFLLGFVLNNNVSMLAEEWRRPQGGQRQKDAAVLRYMFCSMVQRAMIAPAVWVS
Homo sapiens/1-348         57  LLAPPLVLFLLGLVMNNNVSMLAEEWKRPPGRRAKDPAVLRYMFCSMAQRALIAPVVWVA
Caenorhabditis elegans/1-329 61 MFGPTAALLLIGITVNSTTWKLAHGFFFRVRDTRHSWKTTCVSWIEVLIQSSVAPIAWLF
Danio rerio/1-346          56  LIVPPIWFFLLGYVMNNNISVLTEEWKRPVGKRSKDPAVLRYMFSSMTQRALIAPAVWIA
```

*
```
                               120       130       140       150       160
                               .         .         .         .         .
Gallus gallus/1-342        116 VTLLDGKCITCAFCTS....LPVEALGNAS.HHGLPQGEVKRVLARIPCKEIY.DGQELI
Homo sapiens/1-348         117 VTLLDGKCFLCAFCTA....VPVSALGNGSLAPGLPAPELARLLARVPCPEIY.DGDWLL
Caenorhabditis elegans/1-329 121 VVFLDGGYYRCYRSHEFCLISDAILCKNSTILNSYASTS...SFNKISDNGKYCPPCICV
Danio rerio/1-346          116 VTLMDGKSFLCAFSPT....ADLSEFVNES.YQSLSQKELLKIQAKIPCKDIF.EEHEII
```

linker
TMD4   CTH

```
                               170       180       190       200       210       220
                               .         .         .         .         .         .
Gallus gallus/1-342        170 ANEVAVRYLRCISQALGWCFVLLMTTLAFLVRSLRPCFTQAVFLKSRYWSHYIDIERKLF
Homo sapiens/1-348         172 AREVAVRYLRCISQALGWSFVLLTTLLAFVVRSVRPCFTQAAFLKSKYWSHYIDIERKLF
Caenorhabditis elegans/1-329 178 PNPTDASYLEAESQIYAWGLLLFSGVAAFLVITCNRMCDKYTLVQRQYVETYKNVETQKF
Danio rerio/1-346          170 SREAATRYIRCLSQACGWTFLMVITLVAFLVRAIRPCFTQAAFLKTKYWSHYIDTERKLF
```

```
                               230       240       250       260       270
                               .         .         .         .         .
Gallus gallus/1-342        230 DETCAEHAKSFAKVCIQQFFQGMSKD.....LTATHCHP..........PRKAPTDAGEA
Homo sapiens/1-348         232 DETCTEHAKAFAKVCIQQFFEAMNHD.....LELGHTNGTLATAPASAAAPTTPDGAEEE
Caenorhabditis elegans/1-329 238 DAVAKEHASQLAEHNARAFFGQKDWTKRDWDWVSGIPEV.................NNPL
Danio rerio/1-346          230 DETCKEHAKSFAKVCIQQYFESISGE.....IVSQLPQSPAKKG..KGNKDEDGEKQKSD
```

```
                               280       290       300       310       320
                               .         .         .         .         .
Gallus gallus/1-342        275 SEKLL...GITDWDTMNIALKSWHRCK......PPLHLHPDA.PHSSNGWAGEWQPHTQP
Homo sapiens/1-348         287 REKLR...GITDQGTMNRLLTSWHKCK......PPLRLGQEEPPLMGNGWAGGG......
Caenorhabditis elegans/1-329 281 FARLRLIAAEKTQQTMYTPLQLWNDNKGYRIPQPDLQLTQIIVDETKED...........
Danio rerio/1-346          283 EERLL...GIRKEGDMNKVLWNWHTCK......PPLLLSKRTEEMNGHA.....HLDTHS
```

```
                               330       340
                               .         .
Gallus gallus/1-342        325 HTQPPAPRREAVAYYSGV..
Homo sapiens/1-348         332 ...PRPPRKEVATYFSKVGS
Caenorhabditis elegans/1-329   ...................
Danio rerio/1-346          329 LTDERHTKKKAVVYYSKV..
```

Supplementary Figure. 1. Sequence alignment of CALHM1 orthologues A multiple sequence alignment of CALHM1 orthologues (*Gallus gallus, Homo sapiens, Caenorhabditis elegans and Danio rerio*). Red boxes indicate identical residues and red characters indicate similar residues. The positions of the TMD1-4 (red bars above the alignment), the CTH (the grey bar above the alignment), and the 'linker' are based on the chCALHM1 structure from the current study. An asterisk and an arrow annotate Asp120 and the position of Pro86 in *Homo sapiens* CALHM1 (Glu85 in chCALHM1), respectively. The multiple sequence alignment was generated using Clustal Omega and graphically presented using ESPript 3.0.
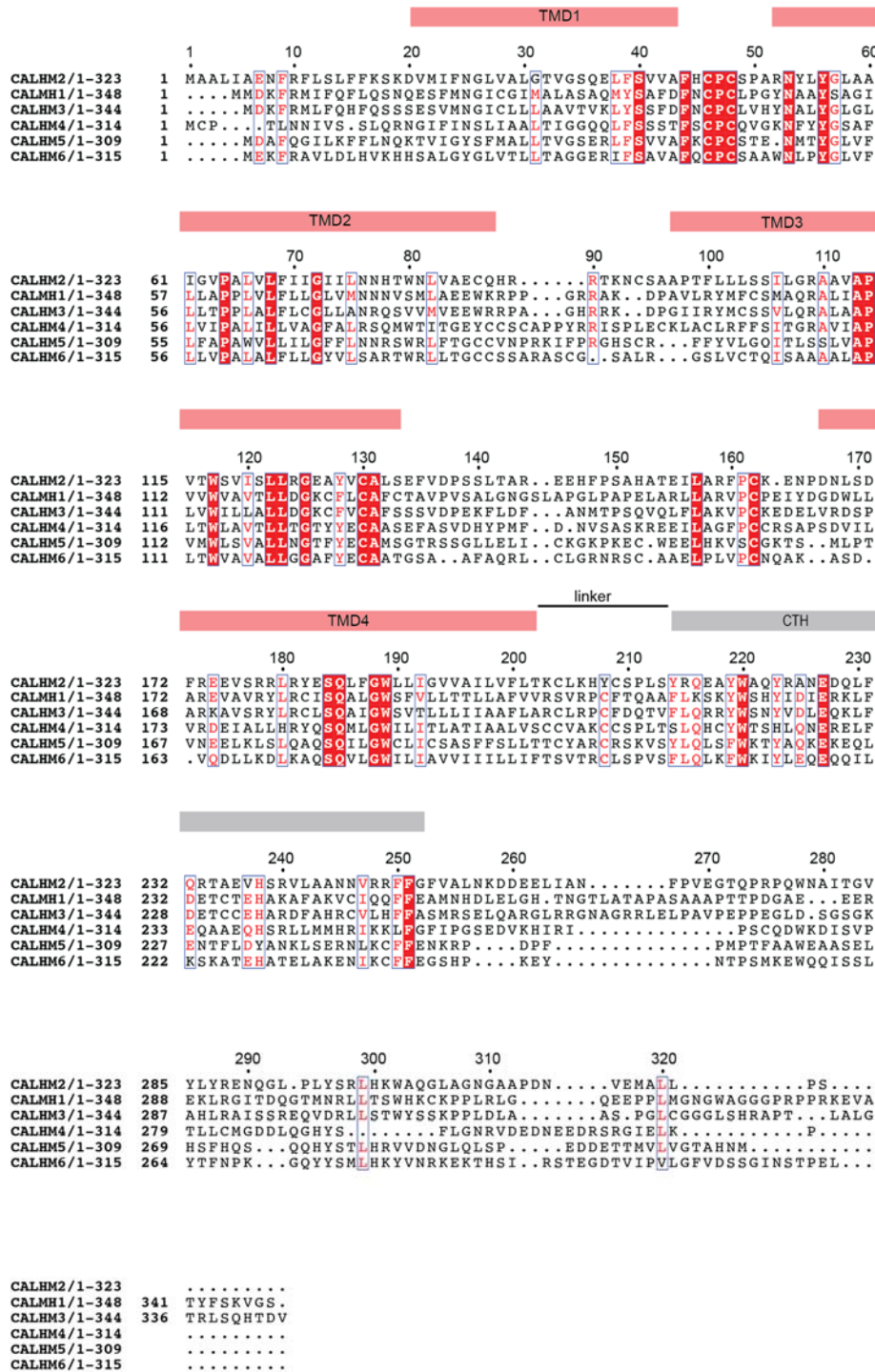
Supplementary Figure. 2. Sequence alignment of CALHM family members. A multiple sequence alignment of the *Homo sapiens* CALHM 1-6. The red boxes indicate identical residues and red characters indicate similar residues. The positions of the TMD1-4 (red bars above the alignment), the CTH (the grey bar above the alignment), and the 'linker' are based on the hCALHM2 structure from the current study. The multiple sequence alignment was generated as in Supplementary Figure. 1.